Journal of Asian Earth Sciences 204 (2020) 104578

Contents lists available at ScienceDirect

Journal of Asian Earth Sciences

journal homepage: www.elsevier.com/locate/jseaes

Detrital zircon U-Pb ages and Hf isotopes of Lower-Middle Devonian to Middle Jurassic sandstones in the Qinfang basin, southern South China block: Constraints on provenance and tectonic setting

Tongbin Shao [a,*], Yun Zhou [b,*], Yongfeng Cai [b], Xinquan Liang [a], Maoshuang Song [a]

[a] State Key Laboratory of Isotope Geochemistry, Guangzhou Institute of Geochemistry, Chinese Academy of Sciences, Guangzhou 510640, China

[b] Collaborative Innovation Center for Exploration of Hidden Nonferrous Metal Deposits and Development of New Materials in Guangxi & Guangxi Key Laboratory of Hidden Metallic Ore Deposits Exploration, Guilin University of Technology, Guilin 541004, China

ARTICLE INFO

Keywords:
Qinfang basin
Provenance
Tectonic setting
Detrital zircon
Paleo-Tethyan Ocean
East Gondwana

ABSTRACT

The affinity and tectonic setting of the Qinfang basin have long been an enigma. Here we conduct detrital zircon U-Pb geochronology and Hf isotope analysis of Lower-Middle Devonian to Middle Jurassic samples from the basin. Along with published age data and paleontology from the basin and its east and west sides, this study constrains the sediment provenance and tectonic setting of the basin. Sandstones of Devonian-Jurassic exhibit an age distribution with major age groups at 2700–2300 Ma (absence for Jurassic), 1200–800 Ma, 600–400 Ma, and 334–246 Ma (for Jurassic alone). Zircons (peak ~2500 Ma) were sourced from the Yangtze block, while ~1200–800 Ma grains may originate from the Yunkai massif and Jiangnan orogen. ~600–400 Ma zircons came from Yunkai massif and/or Cambrian to Silurian sediments in the basin. Carboniferous-Early Triassic (334–246 Ma) zircons were probably supplied by an older sequence in the Great Youjiang basin and the Darongshan-Shiwandashan igneous rocks. The Qinfang basin and its two sides are considered to share a common East Gondwana source in Silurian. The similarity in age spectra between Silurian-Devonian samples in the basin and Ailaoshan belt suggests that the basin is a remnant of the Paleo-Tethyan (Ailaoshan) Ocean. However, the distinct age distribution between the basin and Indochina block shows that the basin is not a part of the Indochina block. By Middle Jurassic following the final closure of the Ailaoshan Ocean in the Late Triassic, the adjacent western area may be still tectonically active, thereby feeding the basin with detritus of Early Permian.

1. Introduction

The South China block (SCB), one of the main continental pieces derived from Gondwana (e.g., Metcalfe, 2013), was formed by the amalgamation of the Cathaysia block to the southeast with the Yangtze block to the northwest during early Neoproterozoic (Fig. 1). After that, the first Phanerozoic orogenic activity, which was termed different names in different studies [such as “Kwangsian movement” in Ting (1929), “early Paleozoic orogeny” in Faure et al. (2009) and Charvet (2013), or “Wuyi-Yunkai orogeny” in Li et al. (2010)], occurred in the early Paleozoic. The orogenic activity plays a significant role in the evolution of the SCB. The effects of this orogeny on the SCB were mainly reflected by an extensive granite intrusion during 460–400 Ma in the Cathaysia block, a regional large-scale angular unconformity between the Devonian cover and metamorphosed pre-Devonian strata, and pervasive deformation and metamorphism in the Cathaysia block and adjacent Yangtze block (Li et al., 2010; Wang et al., 2011a, 2012a, 2013a; Charvet et al., 2010; Shu et al., 2008, 2015). To date, there is no evidence suggesting that there is a relict early Paleozoic ocean in the SCB. Also, the abrupt change in the sedimentary facies occurred from the Yangtze to Cathaysia blocks. Both them were invoked to suggest that intracontinental deformation, rather than oceanic subduction, led to this orogenic event (Faure et al., 2009, 2014, 2016; Charvet, 2013; Charvet et al., 2010; Ren and Li, 2016; Shu et al., 2014; Wang et al., 2010a, 2013a).

Interestingly, recent studies suggested a disparity that Silurian sequences within the Cathaysia block are only present in the Qinfang basin of the southern Cathaysia block but absent in its adjacent areas (Figs. 2,

* Corresponding authors at: State Key Laboratory of Isotope Geochemistry, Guangzhou Institute of Geochemistry, Chinese Academy of Sciences, Kehua Street, Guangzhou 510640, China, and College of Earth Sciences, Guilin University of Technology, No. 12, Jiangan Road, Guilin 541004, China.

E-mail addresses: tshao@gig.ac.cn (T. Shao), zhouyun@glut.edu.cn (Y. Zhou).

https://doi.org/10.1016/j.jseaes.2020.104578
Received 8 June 2020; Received in revised form 6 October 2020; Accepted 6 October 2020
Available online 13 October 2020

3; Zhang et al., 2018; Xu et al., 2014a and references therein), which has long puzzled researchers' understanding regarding the early Paleozoic geology of South China (Zhang et al., 2018). Furthermore, a lot of debates are present concerning the tectonic setting of the Qinfang basin, of which one popular dispute is that the basin is considered either a residual Cambrian ocean (e.g., Li et al., 1994; Liu and Xu, 1994) or a portion of an intracontinental basin within the Cathaysia block (Wang et al., 2010a; Yao and Li, 2016). Another dispute is regarding the tectonic affiliation. The basin was considered to belong to either the Indochina block (Cai and Zhang, 2009) or the SCB (e.g., Yao and Li, 2016; Zhang et al., 2018) during the early Paleozoic.

Recently, Xu et al. (2017) suggested that the Qinfang basin is not a remnant of the Paleo-Tethyan (Ailaoshan) Ocean. One important reason is that age distributions of detrital zircons in the Qinfang basin and the Ailaoshan belt from the Silurian strata are similar, but those from the Devonian strata are distinct. However, there is only one Devonian sample (68 detrital zircons) analyzed in their study, which is not enough to represent the Devonian strata in the basin as local non-uniformity or insufficient analyses may be present. For example, one Devonian sample analyzed by Zhang et al. (2018) displayed a different age distribution of detrital zircons with that reported in Xu et al. (2017). Furthermore, this is also true for the Silurian sample of the Qinfang basin reported in these two studies (Xu et al., 2017; Zhang et al., 2018). Concerning the discrepancies, the source of detrital zircon and the tectonic affinity of the basin reported previously may be questionable. Therefore, it is necessary to perform a further study on detrital zircons and integrate all data to make the age distribution of detrital zircon from related strata more representative.

Here, we investigate the detrital zircon U-Pb ages and Hf isotopes of Lower-Middle Devonian to Middle Jurassic sandstones from the Qinfang basin (Figs. 2 and 3). Combining with the previous age and Hf isotope data, we compare the sediment provenance between the Qinfang basin and its east and west sides and discuss depositional ages and provenance, thereby constraining the affinity and tectonic setting of the basin.

2. Geological background

2.1. South China block

A large number of studies have come to a consensus that the SCB was formed through the welding of the Cathaysia with Yangtze blocks along a boundary forming the Jiangnan orogen during early Neoproterozoic (Fig. 1; Cawood et al., 2013; Li et al., 2002, 2007; Shu et al., 2011; Wang et al., 2013b; Ye et al., 2007), although both the time (e.g., ~440 Ma, Peng et al., 2016a, 2016b; 0.86–0.83 Ga, Wang et al., 2007a; Shu et al., 2011; 0.90–0.88 Ga, Li et al., 2003; Wang and Li, 2003; ~1.0–0.9 Ga, Li et al., 2002, 2007; ~1.9 Ga, Dong et al., 2015) and the way (either single- or double-sided subduction) of the welding (e.g., Cawood et al., 2013; Zhao, 2015) are controversial. The boundary appears roughly parallel to the Jiangshan-Shaoxing fault zone and associated structures (Charvet et al. 2010), but it is unclear in its southwestern extension (Fig. 1). After welding, the intraplate deformation history with three

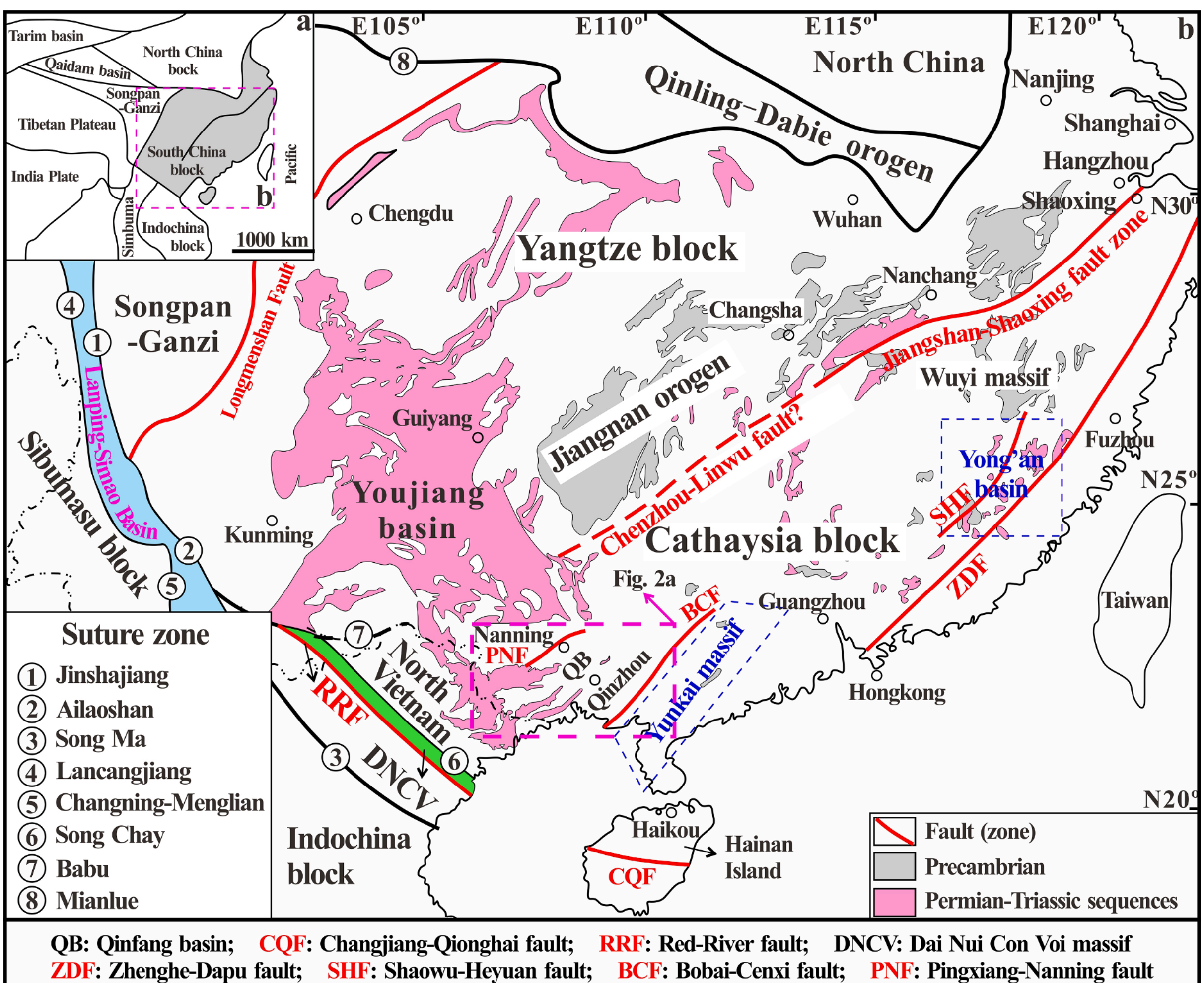

Fig. 1. (a) Main tectonic elements of East Asia (modified from Metcalfe, 2006). (b) Simplified geological map of the South China block (based on the 1:5,000,000 geological map of China), in which the boundary of the Jiangnan orogen and Jiangshan-Shaoxing fault zone is from Li et al. (2008a) and Cawood et al. (2013).

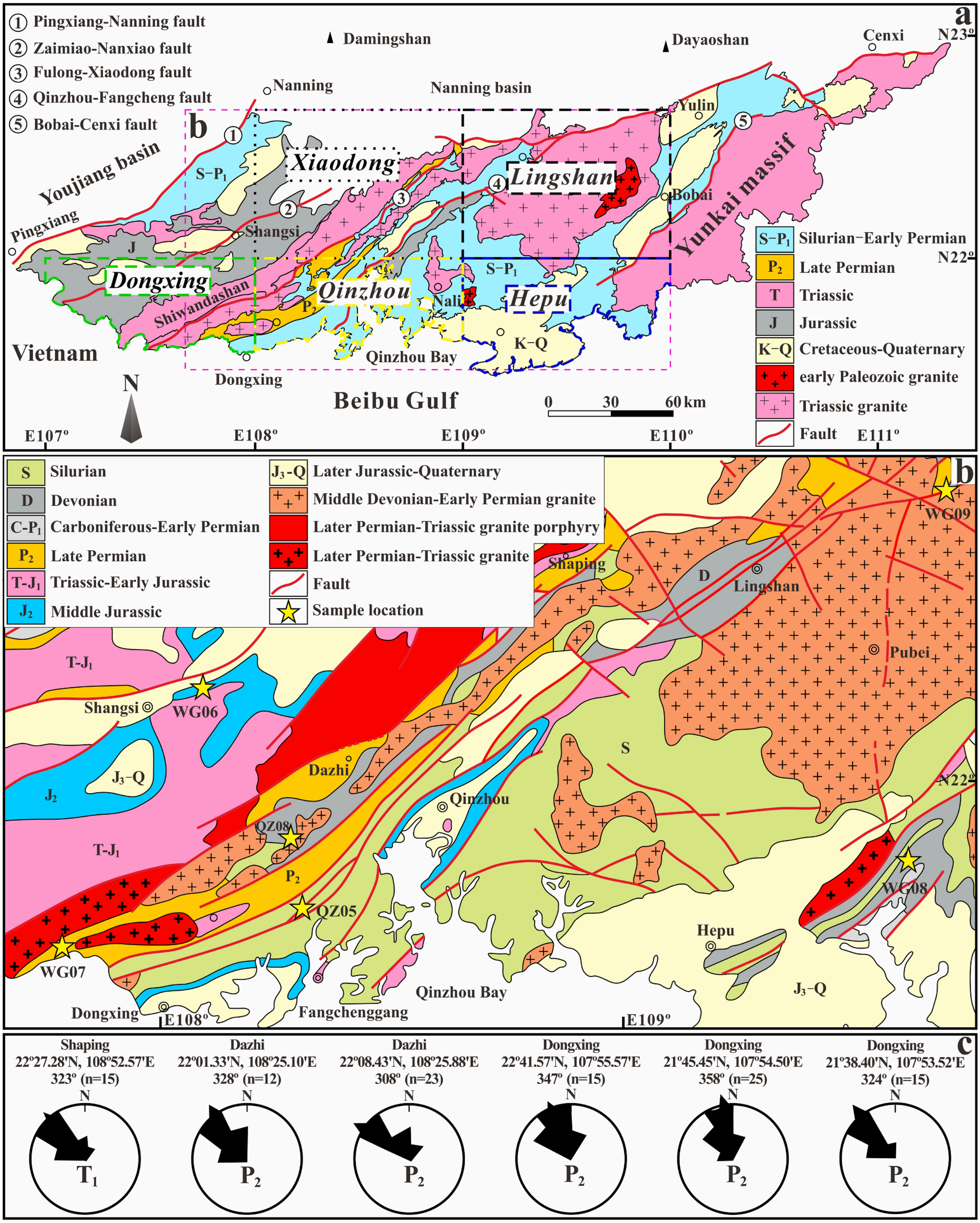

Fig. 2. (a) Geological map for the Qinfang basin (modified from 1:200,000 Qinzhou geological map, Regional Geology of Guangxi Zhuang Autonomous Region). Italics *Dongxing* (bounded in green dashed line), *Xiaodong* (in black dotted line), *Qinzhou* (in yellow dashed line), *Hepu* (in blue dashed line), and *Lingshan* (in black dashed line) represent the locations where five stratigraphic columns drawn in Fig. 3 were labeled. The region that consists of these five areas roughly corresponds to the Qinfang basin. (b) Study area in the Qinfang basin showing the sampling locations of this study. (c) Paleocurrent rose diagrams for the Upper Permian to Lower Triassic succession (data from Liang and Li, 2005).

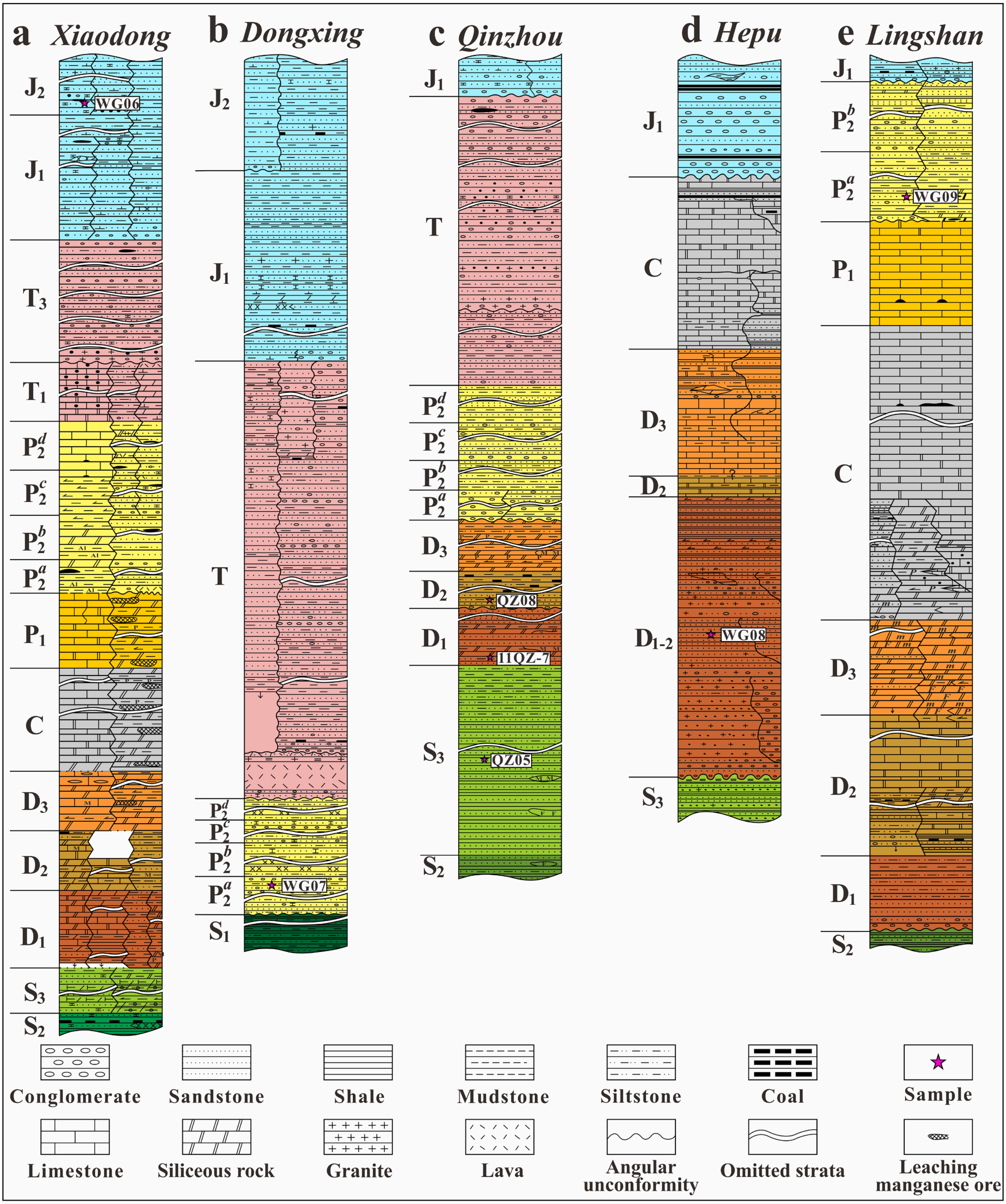

Fig. 3. Schematic stratigraphic columns across the Qinfang basin. The red stars show sampling locations of samples WG06, WG07, WG08, and WG09 from this study, and of samples QZ05 and QZ08 from Zhang et al. (2018) and 11QZ-7 from Xu et al. (2017). Columns a-e are in turn redrawn after 1:200,000 geological maps of the Xiaodong, Dongxing, Qinzhou, Hepu, and Lingshan areas.

orogenic events during different periods (i.e., Jurassic-Cretaceous, Permian-Triassic, and early Paleozoic) dominated the Phanerozoic development and the present configuration of South China (Charvet et al., 2010; Li et al., 2016; Lin et al., 2008; Shu et al., 2014, 2015; Wang et al., 2013a). Of these orogenic events, the most significant tectono-thermal event occurred in the Permian-Triassic, represented by the convergences between the NCB and SCB along the Qinling-Dabie orogen (e.g., Hacker et al., 1998; Meng and Zhang, 2000; Dong et al., 2011), between the SCB and Indochina block along the Ailaoshan-Song Ma suture zone (Lepvrier et al., 2008; Cai and Zhang, 2009; Faure et al., 2014), and between the Sibumasu and Indochina blocks along the Sukhothai zone (Arboit et al., 2014; Carter et al., 2001). These convergences resulted in the closure of the Paleo-Tethys Ocean (Metcalfe, 2013). However, there is another view that the flat subduction of the Paleo-Pacific plate beneath the Eurasian plate during the Permian-Triassic transitional period made the SCB, especially its eastern portion to be evolved into an Andean-type active margin (Li and Li, 2007; Li et al., 2012).

In addition to Jiangnan/Sibao orogen formed from a metaigneous and metasedimentary Neoproterozoic assemblage (Qiu et al., 2000; Zhao and Cawood, 2012), there is a spatially limited and poorly exposed Archean and Paleoproterozoic basement in the SCB. This antique basement is unconformably overlain by both a middle-upper Neoproterozoic and lower Paleozoic succession, which are accumulated in an aulacogen environment (i.e., Nanhua and Kangdian rifts; Cawood et al., 2018; Shu et al., 2008, 2011; Wan, 2010; Wang and Li, 2003; Wang et al., 2012a; Zhao and Cawood, 2012). Mesoarchean to early Paleoproterozoic (~3200–2300 Ma) gneisses and amphibolites are found to be exposed in the Kongling complex of the Yangtze block (e.g., Qiu et al., 2000; Zhao and Cawood, 2012). In contrast, late Paleoproterozoic (~1800 Ma) metamorphic rocks are mainly distributed in the Wuyi massif of the Cathaysia block (Fig. 1b; Yu et al., 2009 and references therein). The next younger rocks are Mesoproterozoic (1600–1400 Ma) rocks confined to Hainan Island and composed mainly of granodiorites (Li et al., 2008b). The youngest Precambrian successions, which are dominated by early to middle Neoproterozoic igneous rocks, are found to distribute along the Jiangnan orogen and around the western margin of the Yangtze block (Fig. 1; Cawood et al., 2013; Wang et al., 2013b).

2.2. Qinfang basin

Tectonically, the Qinfang basin is bounded by the Pingxiang-Nanning fault and Devonian to Middle Triassic Youjiang basin to the northwest (Yang et al., 2012), by the Bobai-Cenxi fault and Yunkai massif to the southeast, and by the Beibu Gulf and the South China Sea to the southwest (Figs. 1 and 2a; BGMRGP, 1988). To the northeast, however, the basin extends into the interior of the Cathaysia block, resulting in a V-shaped region (e.g., Zhang et al., 2018). The basin is filled with strata from the bottom of Lower Silurian to Lower Jurassic, in which several unconformities occurred throughout the basin (Fig. 3). The Lower-Middle Devonian Guitou Group ($D_{1\text{-}2}gt$) in Hepu area, which has a conformable relationship with the overlying Middle Devonian Donggangling Formation (D_2d) and an angular unconformability with the underlying Upper Silurian, consists primarily of light-gray thick-bedded coarse-grained sandstone with intercalated fine-grained sandstone at the top, and yellowish-white or light-grey basal conglomerate, fine-grained conglomerate, conglomeratic sandstones and medium-coarse grained sandstone at the bottom (Fig. 3d). The lower part of the Upper Permian sequence in Pubei area, which is overlain conformably by the upper part of the Upper Permian sequence and has an unconformable relationship with the underlying Lower Permian Maokou Formation, is composed mainly of grey-green mudstone, silty mudstone, argillaceous siltstone, sandstone, with gravel-bearing coarse-grained sandstone and intercalated gravel sandstone at the bottom (Fig. 3e). The first formation of the Upper Permian in Dongxing area, which is conformably overlain by the second formation of the Upper Permian and angular unconformably underlain by the forth formation of the Lower Silurian Liantan Group, is characterized by gray thick-bedded conglomerate and pebbly sandstone with intercalated silty mudstone at the top, sediment hiatus in the middle portion, and interbeds of unequal-grained sandstone and silty mudstone intercalated pebbly-bearing clastic sandstone at the bottom (Fig. 3b). The Middle Jurassic Nadang Group in Shangsi area, which is conformably overlain by the Upper Jurassic and underlain by the Lower Jurassic Baixing Formation, contains mica and argillaceous siltstone, calcareous siltstone with granitic sandstone in the upper portion, sediment hiatus in the middle portion, and lithoclastic sandstone and peddled lithoclastic sandstone sandwiched with coal lines in the lower portion (Fig. 3a).

According to Liang and Li (2005), the strata from the Upper Permian to Lower Triassic are considered to record the change from the foreland basin to Indosinian orogen further south (e.g., Cai and Zhang, 2009; Hu et al., 2015a; Tang et al., 2013; Zhao et al., 2010, 2012). As shown in Fig. 2, middle Paleozoic-early Mesozoic granites occur widely in this basin. The Paleozoic succession, which is conformable and composed of siliciclastic Paleozoic strata that display a fault contact relationship with the northern Mesozoic-Cenozoic Nanning basin, are mainly exposed in the central and eastern portions of the Qinfang basin (i.e., Qinfang area), while the Mesozoic succession is found to appear principally in the western portion (i.e., Shiwandashan area) (Fig. 2; BGMRGZAR, 1985). Capping the Paleozoic-Lower Triassic foreland succession, a basin-throughout Middle Triassic unconformity corresponds to an extensive emplacement into the pre-Middle Triassic succession (Fig. 2a; BGMRGZAR, 1985) of Indosinian S-type granite (240–230 Ma, Zhao et al., 2010).

2.3. Yunkai massif, Hainan Island and northeast Vietnam terrane

The NE/ENE-trending Yunkai massif, located in eastern Guangxi and western Guangdong Provinces, represents a crystalline basement adjoining to the Qinfang basin (Figs. 1b and 2a). It is an important tectonic zone that experienced a strong Kwangsian tectono-magmatic event, which is characterized by ~460–430 Ma *syn*-orogenic crustal thickening and ~430–400 Ma post-orogenic extension (Charvet et al., 2010; Li et al., 2010; Shu et al., 2015; Wang et al., 2012a, 2013b). The base of the massif is widely occupied by Paleoproterozoic metamorphic complexes (BGMRGZAR, 1985; BGMRGP, 1988; Zhang et al., 2012), which have an unconformable contact with overlying pelagic/hemi-pelagic deposits of Sinian and lower Paleozoic. All these strata and rocks were intruded by granites of the early Paleozoic (465–395 Ma) and Permo-Triassic (270–230 Ma) ages and were influenced by later tectono-thermal activities (BGMRGP, 1988; Peng et al., 2006; Wang et al., 2007b; Lin et al., 2008; Zhang and Cai, 2009; Wang et al., 2011a). Together with the northern Hainan Island (Zhang and Cai, 2009), this massif forms the portion of the Precambrian basement of the Cathaysia block (e.g., Yu et al., 2010; Zhao and Cawood, 2012).

Locating near the southern end of the South China mainland and to the southeast of the Qinfang basin (Fig. 1), appearing is Hainan Island, which is composed of a basement including Neoproterozoic sedimentary units (BGMRGP, 1988; Yao et al., 2017) and early Mesoproterozoic (1600–1400 Ma) igneous (Li et al., 2008b) and sedimentary rocks. Overlying the basement of the island are Paleozoic to Mesozoic strata (Xu et al., 2014b; Zhou et al., 2015). Mesoproterozoic rocks also occur in the western Yangtze block (e.g., the Dongchuan Group; Wang and Zhou, 2014), certainly not just on Hainan Island. Additionally, it also underwent Permian-Triassic tectono-thermal events (Tang et al., 2013; Xie et al., 2006; Xu et al., 2007).

Similarly, the northeast Vietnam terrane is also characterized by a Precambrian metamorphic basement (e.g., Chen et al., 2014), overlying of which is a series of Paleozoic-early Mesozoic magmatic and metamorphic rocks (Chen et al., 2014; Faure et al., 2014; Vuong et al., 2013; Yan et al., 2006). The south margin of the terrane is marked by the Song Chay ophiolitic mélange, which is considered to record the convergence and collision of the SCB with the Indochina block (e.g., Faure et al., 2014; Lepvrier et al., 2008).

3. Sampling

In this paper, four sedimentary rock samples for detrital zircon analysis were collected from the Lower-Middle Devonian to Middle Jurassic strata of Qinfang basin, within which a disconformity takes place between Upper and Lower Triassic strata due to the Indosinian orogeny (Figs. 2 and 3). The Permian and Triassic sedimentary sequences are absent in the Hepu area (Fig. 3d). Sample WG06 was collected from the Middle Jurassic (Nadang Group) in the Shangsi area (shown in stratigraphic column of Xiaodong, Fig. 3a) of the western Qinfang basin. Samples WG07 and WG09 were collected from the first formation of the Upper Permian in the Dongxing area of the southwest Qinfang basin and the lower part of the Upper Permian in the Pubei area (shown in stratigraphic column of Lingshan, Fig. 3e) of the northeast Qinfang basin, respectively. Lower-Middle Devonian sample WG08 was collected along the road of Gongguan to Quzhang Town, in the Hepu area of the southeast Qinfang basin (shown in stratigraphic column of Hepu, Fig. 3d). Sample WG06 is yellow medium-grained sandstone in which there is ~68% quartz, ~21% feldspar, and ~11% lithic fragments. In contrast, sample WG07 appears gray fine-grained sandstone with ~65% quartz, ~20% feldspar, and ~15% other minerals (such as mica and heavy minerals) contained. Sample WG08, gray-white medium-grained sandstone, consists of ~94% quartz, ~4% lithic fragments, and ~2% feldspar. Upper Permian sample WG09 is also grey fine-grained sandstone composed of ~82% quartz, ~12% lithic fragments, and ~6% mica and heavy minerals.

4. Analytical methods

Zircon grains were extracted from whole-rock samples using heavy-liquid and magnetic separation and then randomly selected by manual hand-picking with the help of a binocular microscope, following which the selected zircon grains were mounted in a thin layer of epoxy resin on petrographic slides and polished down to roughly half sections to expose the interiors. All these processes were designed to prevent or minimize cross-contamination between samples. Cathodoluminescence (CL) imaging and optical observation were combined to inspect the zircon morphology, and the clearest, least fractured rims of the zircon crystals were selected as suitable targets for further *in-situ* analyses. The CL imaging was performed in a JXA-8100 Electron Probe Microanalyzer with a Mono CL3 Cathodoluminescence System at the State Key Laboratory of Isotope Geochemistry (SKLIG), Guangzhou Institute of Geochemistry, Chinese Academy of Sciences (GIGCAS). Zircon U-Pb dating on four samples (i.e., WG06, WG07, WG08, and WG09) and Hf isotopic compositions and trace elements of zircons from samples WG06 and WG08 were obtained using an Agilent 7500a laser ablation ICP-MS instrument in combination with an excimer 193 nm laser ablation system (GeoLas 2005) at the State Key Laboratory of Continental Dynamics (SKLCD), Northwest University, Xi'an, China. The system was employed in relation to an Elan6100 DRC Q-ICP-MS and a Nu Plasma HR MCICP-MS. The following operating conditions were used for all analyses: a 40 μm spot diameter with a 10 Hz repetition rate at 10–15 J/cm^2 energy density. Through a Y-shaped connector, the zircon aerosol generated by the laser was split behind the ablation cell into two transport tubes and concurrently introduced into the two mass spectrometers. Among them, the Q-ICP-MS was employed to determine U–Pb ages, while the MC-ICP-MS instrument was applied to measure trace elements and Hf isotopic compositions. Analytical procedures similar to those described by Liu et al. (2010) and Yuan et al. (2008) were carried out. ICPMSDataCal7.2 (Liu et al., 2008) was used to calculate the U-Pb ages, and then Harvard zircon 91,500 and GJ-1 were used as the external standards for calibration. With the Isoplot program (Ludwig, 2001), concordia diagrams, probability distribution plots, and weighted mean calculations were performed.

According to a decay constant for ^{176}Lu of 1.865E-11 (e.g., Scherer et al., 2001), we calculated the initial ^{176}Hf/^{177}Hf values. It is assumed that a mean ^{176}Hf/^{177}Hf value is 0.015 for the average continental crust (Griffin et al., 2002). Furthermore, present-day ^{176}Hf/^{177}Hf and ^{176}Lu/^{177}Hf ratios of chondrite are 0.282772 and 0.0332, respectively; and those of depleted mantle are 0.28325 and 0.0384, respectively (Blichert et al., 1997; Vervoort and Blichert, 1999). Based on this, we computed the model ages (T_{DM}), which are suitable for grains either derived from juvenile magma produced directly from the depleted mantle or by remelting the material just extracted from the depleted mantle. For this reason, the model ages are believed to represent only the minimum age for the magma source material from which zircon is crystallized. By assuming that parental magma was produced by melting of an average continental crust sourced from the depleted mantle, in contrast, the crustal model ages (T_{CDM}) are considered to reflect the reworking of older crust with juvenile material added (e.g., Belousova et al., 2010). The T_{DM} is characterized by $\varepsilon_{Hf}(t)$ which is at least 0.75 times the ε_{Hf} values of the depleted-mantle curve, while the calculation of T_{CDM} was performed for all other analyses. The U-Pb age and REE data of zircons were also collected for Hf isotope analysis. Using ^{29}Si as the internal calibration, U, Th, and Pb concentrations were corrected.

5. Results

5.1. CL images and Th/U ratios

Representative CL images of the detrital zircons of the four samples along with spot ages are shown in Fig. 4. Some zircons show approximately round grain morphology, which indicates that they have undergone long-distance transportation and abrasion or possible multi-cycled deposition. The other zircon grains are subhedral to euhedral in crystal morphology, suggesting that they experienced short transportation from the source region. Igneous zircons from various rocks are characterized by a Th/U ratio ranging from 0.2 to 1.0, while the metamorphic zircon has a lower Th/U ratio, less than 0.1 (e.g., Kinny et al., 1990). For this reason, the Th/U ratio of zircon is usually employed to distinguish its origin (e.g., Maas et al., 1992). Considering that there may be some exceptions that igneous zircons exhibit a low Th/U ratio and vice versa, it is, therefore, risky to distinguish the metamorphic origin from the igneous origin of zircons in terms of the Th/U ratio alone (Hidaka et al., 2002). Despite this, the Th/U ratios are still effective in making a rough estimate of the origins of zircons. Here, the composition zoning in most zircons is planar or oscillatory, and Th/U ratios of 168 grains among the 241 zircon U-Pb ages are greater than 0.4 (see Fig. 5 and Supplementary Table S1), which indicates that these zircons were sourced from magmatic protoliths. Although slightly high Th/U ratios (Table S1), shiny CL images (Fig. 4; Hidaka et al., 2002) suggest that a few zircons [such as zircon WG06-41 (1003 Ma)] are metamorphic origin, indicating that Mesoproterozoic metamorphism may occur in the source region, thereby providing a metamorphic imprint for the source material for later deposition.

5.2. U-Pb age of detrital zircons

We performed a total of 241 analyses for 241 zircon grains from the four sandstone samples and listed the zircon U-Pb isotopic compositions in Table S1. Analyses in the data table and Concordia plots are reported at a 1σ level. Although all analyses are plotted on Concordia graphs (Fig. 6), only 227 analyses showing discordance lower than 10% are plotted in the frequency distribution histogram (Fig. 7). The ^{206}Pb/^{238}U ratios are used to define U-Pb ages less than 1000 Ma, while the ^{207}Pb/^{206}Pb ratios are applied to older ages. Zircon U-Pb data of the Lower Devonian to Middle Jurassic sandstones yield various groups of ages (Figs. 6 and 7), which means that the Qinfang basin was fed by multiple sources and experienced a complex erosion process.

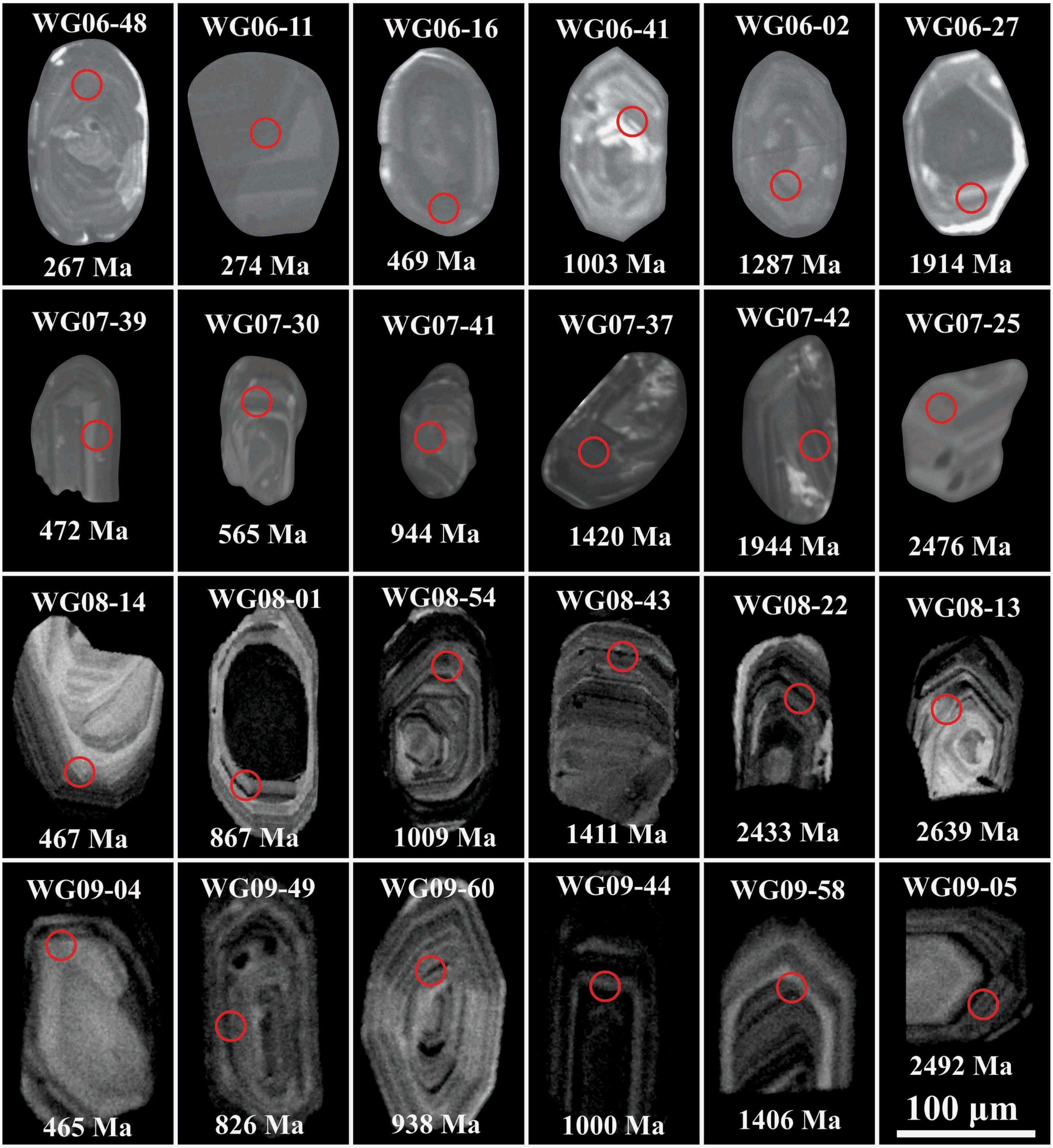

Fig. 4. Representative CL images showing internal structure and morphology of detrital zircons from the Qinfang basin.

Fifty-eight analyses were carried out on sample WG06, among which fifty-three ages ranging from 1914 ± 54 Ma to 246 ± 7 Ma were obtained on or near the concordia curve (Fig. 6a). In this distribution range, the age spectra of the grains with ages of 2000–600 Ma are scattered (Fig. 6a). The age spectra are characterized by three groups. Specifically, group 1 involves 23 grains ranging from 246 Ma to 334 Ma with one prominent peak at 288 Ma, group 2 includes 14 grains from 412 Ma to 599 Ma with one major peak at 471 Ma and mean age at 473 Ma, and group 3 contains 15 grains varying from 679 Ma to 1576 Ma with a subordinate peak at 1000 Ma. Furthermore, the age of 1914 ± 54 Ma was yielded for the oldest grain (Fig. 7a).

Sixty-three zircon grains were selected for sample WG07 to be analyzed, and sixty analyses are shown on or near the concordia curve (Fig. 6b). Ages of these zircon grains vary from 3650 ± 39 Ma to 458 ± 11 Ma, most of which can be divided into five distinct age groups: 458 Ma to 595 Ma (n = 14) with a prominent age peak at 471 Ma and a subordinate age peak at 576 Ma; 808 Ma to 1213 Ma (n = 22) with a major age peak at 988 Ma; 1332 Ma to 1661 Ma (n = 8) with a subordinate age peak at 1447 Ma; the fourth group consisting of three ages of 1936 Ma, 1944 Ma and 1981 Ma with a peak at 1965 Ma and a mean age

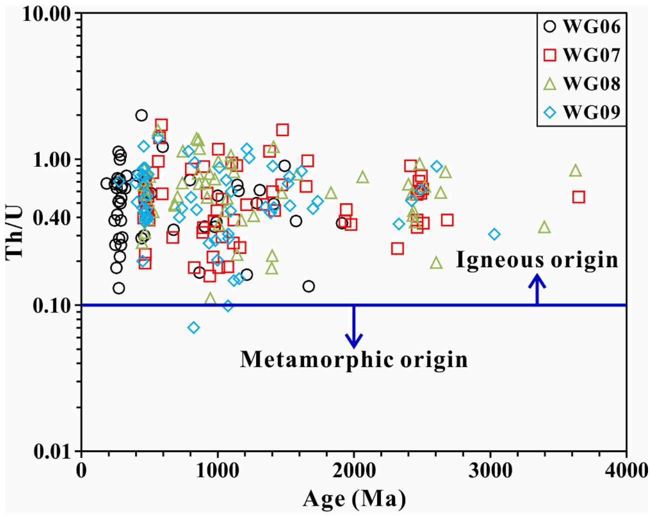

Fig. 5. The plot of Th/U ratios versus age (Ma) for the Lower Devonian-Middle Jurassic sandstone samples from the Qinfang basin.

at 1954 Ma; and the final group including 2321 Ma to 2687 Ma (n = 12) with a dominant age peak at 2482 Ma. Also, a concordant age of 3650 ± 39 Ma was obtained for the oldest grain (Fig. 7b).

Sample WG08 has a frequency distribution similar to that of sample WG07. Analyses of sixty zircon grains yield fifty-six ages on or near the concordia curve (Fig. 6c). The age groups are classified into three ranges: 448 Ma to 563 Ma (n = 14) with a distinct age peak at 471 Ma and the average age at 482 Ma; 686 Ma to 1584 Ma (n = 29) with three subordinate age peaks at 871 Ma, 1012 Ma, and 1412 Ma; 2402 to 2673 Ma (n = 10) with two subordinate ages at 2435 Ma and 2671 Ma. Concordant ages of 3398 ± 25 Ma and 3628 ± 15 Ma were yielded for the two oldest grains (Fig. 7c).

Sixty analyses of zircon grains were conducted for sample WG09, of which fifty-eight analyses are displayed on or near the concordia curve (Fig. 6d). Ages between 401 ± 12 Ma and 3032 ± 44 Ma are yielded for sample WG09. However, there is only one major age group clustered from 401 Ma to 563 Ma (n = 23) with a major age peak at 465 Ma. Between 720 Ma and 1735 Ma (n = 31), there is a relatively dispersive age spectrum with two subordinate age peaks at 826 Ma and 1011 Ma. The rest of four zircon grains display concordant ages of 2331 ± 48 Ma, 2492 ± 42 Ma, 2610 ± 46 Ma, and 3032 ± 44 Ma (Fig. 7d).

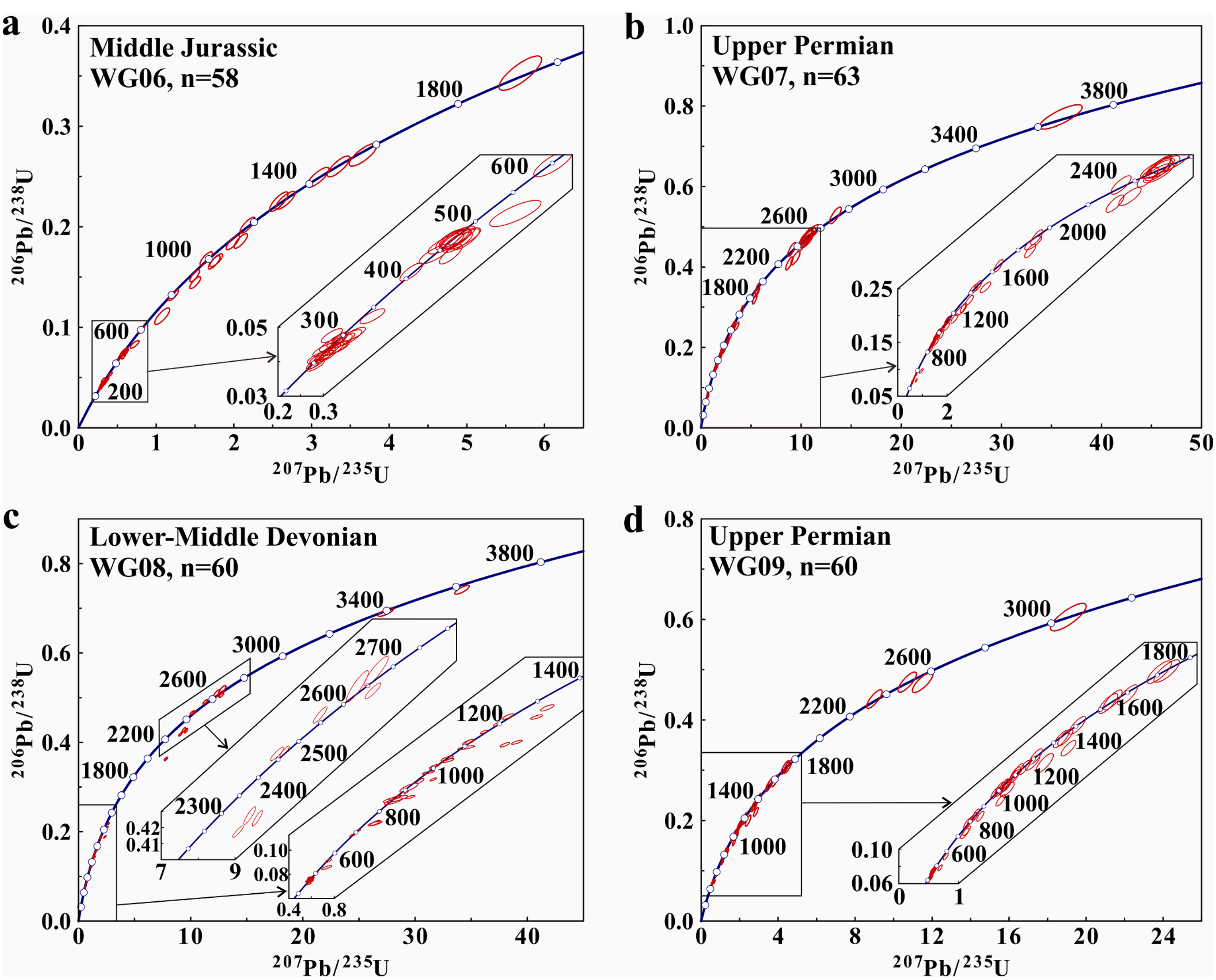

Fig. 6. LA-ICPMS U-Pb concordia age plots for detrital zircons from the sandstone samples from the Qinfang basin.

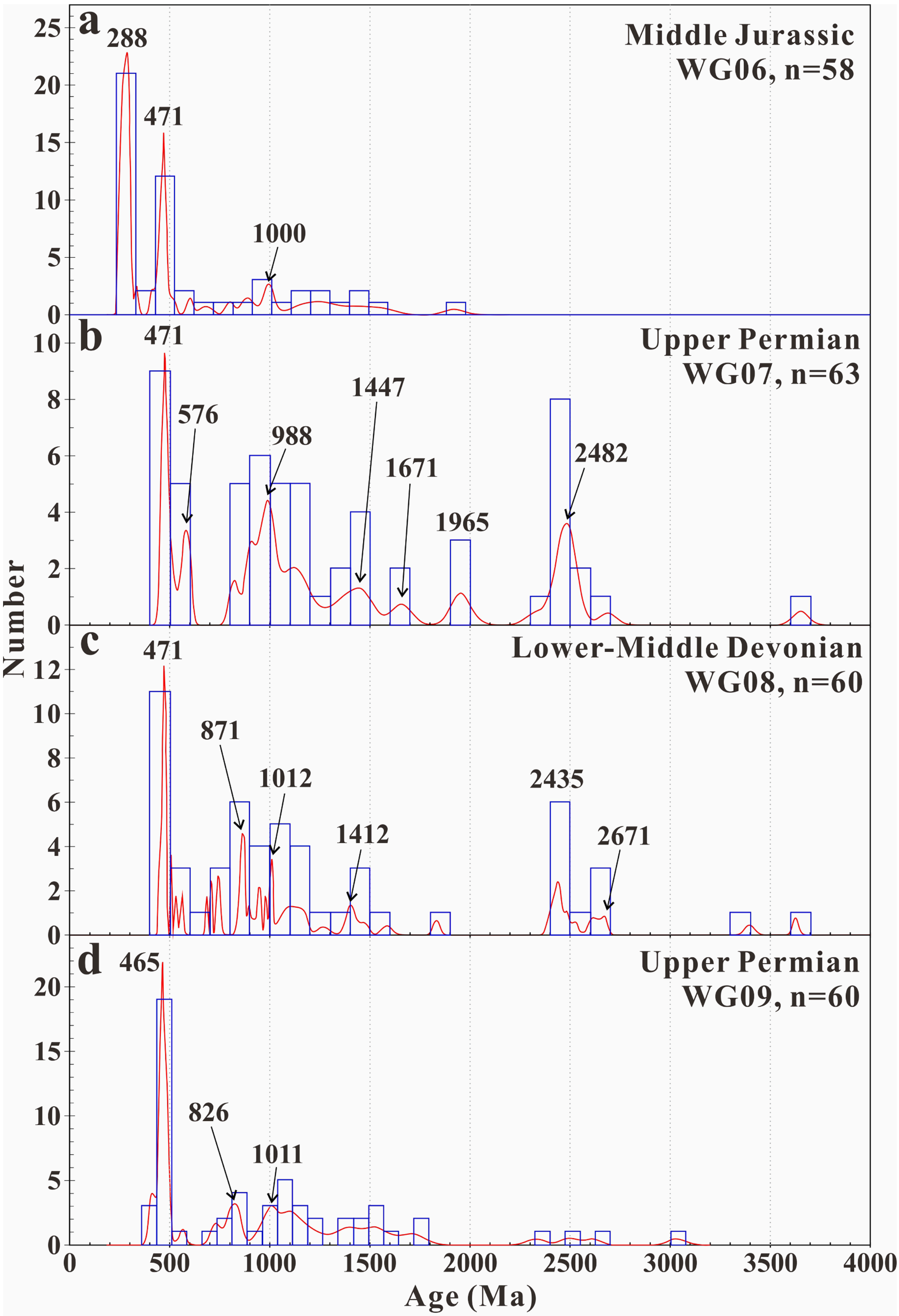

Fig. 7. Probability density plots and age histogram of detrital zircons from the sandstone samples from the Qinfang basin.

5.3. Hf isotopic composition

Hf isotopic composition analyses were performed on zircon grains from both samples WG06 and WG08, and the results are listed in Supplementary Table S2. A wide range of ^{176}Hf/^{177}Hf (0.281249 to 0.282848 and 0.280260 to 0.282683, respectively) and ^{176}Lu/^{177}Hf (0.000257–0.001920 and 0.000030–0.003389, respectively) ratios are shown for the zircons of these two samples.

Fifty-three zircon grains selected from sample WG06 were analyzed for Hf isotopes (Table S2, Fig. 8). Most Cambrian to Triassic (514–246 Ma) detrital zircons show negative $\varepsilon_{Hf}(t)$ values (–0.43 to –47.53), and seven grains embody positive $\varepsilon_{Hf}(t)$ (+2.36 to +8.17) with model ages between 896 Ma and 601 Ma. Three late to middle Neoproterozoic (799–599 Ma) grains exhibit negative $\varepsilon_{Hf}(t)$ values of –15.14 to –26.68 and a positive $\varepsilon_{Hf}(t)$ value of +8.62. In contrast, most zircon grains with middle Mesoproterozoic to early Neoproterozoic ages (1287–869 Ma) yield negative $\varepsilon_{Hf}(t)$ values (–2.59 to –14.26), indicating that these zircons were sourced from crustal materials. In this age range, only one grain shows a positive $\varepsilon_{Hf}(t)$ of +8.27. For ages lying between 1576 Ma and 1311 Ma (late to middle Mesoproterozoic), three zircon grains are characterized by positive $\varepsilon_{Hf}(t)$ values (+0.31 to +4.35) with model ages between 1855 Ma and 1782 Ma, and the only one left has a negative $\varepsilon_{Hf}(t)$ of –8.09 with a model age of 2263 Ma. Besides, one middle Paleoproterozoic (1914 Ma) grain yields a negative $\varepsilon_{Hf}(t)$ of –1.67 with a model age of 2375 Ma.

Hf isotope analyses were carried out on fifty-two dated zircon grains from sample WG08. For detrital zircons with Cambrian to Ordovician ages (529–448 Ma), most yield negative $\varepsilon_{Hf}(t)$ values (–4.17 to –18.39) with model ages between 1824 Ma and 1230 Ma, and only one grain shows a positive $\varepsilon_{Hf}(t)$ of +8.33 with a model age of 796 Ma. Among twenty-seven early Mesoproterozoic to late Neoproterozoic (1584–563 Ma) zircon grains, twenty-three grains yield negative $\varepsilon_{Hf}(t)$ values (–1.02 to –39.11) with model ages varying from 2946 Ma to 1622 Ma, and the other four zircons display positive $\varepsilon_{Hf}(t)$ values (+2.55 to +3.85) with model ages of 1793–1109 Ma. One late Paleoproterozoic (1833 Ma) grain exhibits a negative $\varepsilon_{Hf}(t)$ of –23.32 with a model age of 3118 Ma. Six early Paleoproterozoic (2483–2402 Ma) zircon grains embody negative $\varepsilon_{Hf}(t)$ values (–0.01 to –13.09) with a mean value of –4.48 and model ages varying from 3249 Ma to 2766 Ma. Four Neoarchean (2673–2522 Ma) grains display $\varepsilon_{Hf}(t)$ ranging from –4.51 to –10.71 with a mean of –7.92. Additionally, two older Archean zircon grains with ages of 3398 Ma and 3628 Ma have $\varepsilon_{Hf}(t)$ of –10.42 and –9.39, respectively (Table S2, Fig. 8).

6. Discussion

6.1. Variation in age spectra with depositional ages

The analyses on detrital zircons of Lower-Middle Devonian to Middle Jurassic sandstones from the Qinfang basin yield a similar range of late Neoproterozoic- to Lower Devonian-aged grains and late Mesoproterozoic- to early Neoproterozoic-aged grains, but late Paleozoic- to early Mesozoic-aged grains are only present in the Jurassic sample WG06 (Fig. 7).

Except for the Jurassic sample, all samples have zircon grains older than 2.3 Ga. Neoarchean-early Paleoproterozoic ages are concentrated between 2.7 and 2.3 Ga, with a major age peak at ~2.5 Ga in both samples WG07 and WG08 and a subordinate age peak at ~2.7 Ga in sample WG08. Late Paleoproterozoic-early late Paleozoic zircon grains in the range of 1.9–0.4 Ga occur in all samples, of which samples WG06 and WG09 display a similar scatter and a subdued peak at ~1.0 Ga, while samples WG07 and WG08 exhibit a similar distribution and several distinctly subordinate peaks. Even so, all samples display a prominent age peak at ~471 Ma.

Late Paleozoic-early Mesozoic zircon grains are present only in the Jurassic sample and absent from the Devonian and Permian sequences (Fig. 7). This fact suggests that the sources feeding the Qinfang basin varied during the Devonian to Jurassic, implying that the basin was located in a tectonically active setting and was fed by continuous sedimentation during that period although local interruptions occurred (Fig. 3).

6.2. Provenance of Lower-Middle Devonian to Middle Jurassic successions in the Qinfang basin

As shown in Fig. 7, 241 zircon grains from the four Lower-Middle Devonian to Middle Jurassic sandstone samples in the Qinfang basin show a broad age range of 3650–246 Ma with major peaks centered at 2700–2300 Ma and 1200–800 Ma for samples WG07 and WG08, 600–400 Ma for all samples, and 334–246 Ma for sample WG06. The difference in age distribution between Upper Permian samples WG07 and WG09 may be associated with either local non-uniformity or

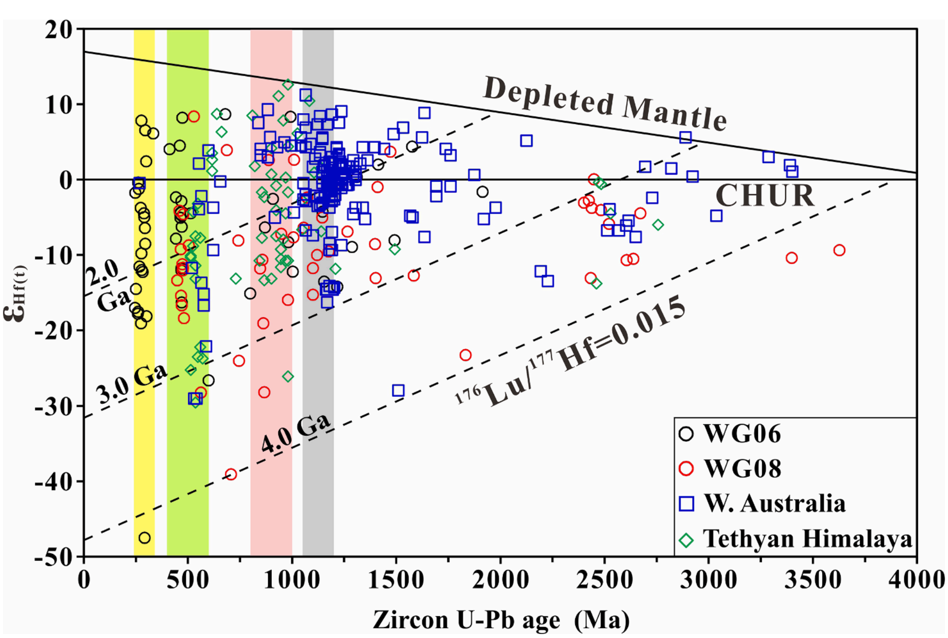

Fig. 8. Plots of crystallization age versus $\varepsilon_{Hf}(t)$ for the detrital zircons from the Qinfang basin (this study), Western Australia (Veevers et al., 2005), and Tethyan Himalaya zone (Zhu et al., 2011). Hf-isotope evolution line for Depleted Mantle is after Griffin et al. (2000). The 240–340 Ma, 400–600 Ma, 800–1000 Ma, and 1050–1200 Ma age groups are shown in yellow, green, pink, and grey bars, respectively. CHUR: Chondritic Uniform Reservoir; dashed lines show the evolution of crustal volumes with ^{176}Lu/^{177}Hf = 0.015, corresponding to the average continental crust.

insufficient analyses (Fig. 7). This local non-uniformity or insufficient analyses may also occur in Devonian samples from the Qinzhou area [11QZ-7 in Xu et al. (2017); Figs. 3c and 9h] and its adjacent Hepu area (WG08 in this study; Fig. 3d and 9g). In contrast, the similarity in age distribution among some samples suggests a possible common source. For example, samples WG07 and WG08 were collected from the Upper Permian and Lower-Middle Devonian sequences, respectively, both which directly angular unconformity overlies Silurian strata (Fig. 3). In these two samples, analyzed Neoarchean-early Paleoproterozoic zircon grains with a peak of ~2500 Ma are found rounded with a rim-core structure and oscillatory zoning (Fig. 4), which means that they have suffered long-distance transportation from their source region and/or multi-cycled sedimentary processing before their deposition. It was reported that Archean igneous rocks were exposed in the Yangtze block (e.g., Cawood et al., 2020; Peng et al., 2009; Zhao et al., 2020) rather than the Cathaysia block. For example, Archean rocks have been recently documented in the Cuoke area of the southwestern Yangtze block (Cawood et al., 2020; Zhao et al., 2020), which is immediately adjacent to the north of the Qinfang basin. Furthermore, detrital zircons of Archean were also widely distributed in metasedimentary rocks and pre-Permian clastic rocks in the Yunkai massif (Qin et al., 2006; Yu et al., 2010). Combined with the studies by Li et al. (2008a) and Qin et al. (2006), the Yunkai massif, along with Hainan Island, was likely to feed the basin with the Paleoproterozoic (1900–1600 Ma) and Mesoproterozoic (1400–1200 Ma) zircons during Early-Middle Devonian to Late Permian. Interestingly, zircon grains with these ages were once reported in Middle Triassic samples from the Youjiang basin (e.g., Yang et al., 2012), northwest of the Qinfang basin. Considering that significant age groups of ~1900–1700 Ma and ~1300–1100 Ma were reported in the Proterozoic metasediments in Yunnan Province, which is right to the northwest of the Youjiang basin (Wang et al., 2011b). Thus, the metasediments may be a source feeding the Youjiang basin. However, this derivation cannot be determined because of no available paleocurrent data. For the same reason, it is uncertain that the Paleoproterozoic-Mesoproterozoic grains in the two samples (WG07 and WG08) were sourced from the metasediments. Besides, the two samples are post-orogenic and are characterized by age distribution similar to the post-orogenic sample from the Middle Devonian strata (Fig. 9f; Zhang et al., 2018) and *syn*-orogenic samples from the underlying Silurian strata (Fig. 9j-l; Xu et al., 2017), but distinct from the *syn*-orogenic samples from the underlying Lower Devonian [sample 11QZ-7 in Xu et al. (2017); Fig. 9h] and Upper Silurian [sample QZ5 in Zhang et al. (2018); Fig. 9i] strata. These samples (i.e. 11QZ-7 and QZ5), collected from the Qinzhou area where the Lower Devonian strata are conformable with the underlying Upper Silurian strata (Fig. 3c), are found to lack early Paleozoic (~500–400 Ma) zircons but possess a pattern of Precambrian (~1000–900 Ma) detrital zircon ages. This Precambrian pattern is similar to that of both the late Neoproterozoic sediments (Yu et al., 2008, 2010) and the early Neoproterozoic igneous rocks (Wang et al., 2013b; Zhang et al., 2012) of the Yunkai massif. This fact suggests that the Yunkai massif fed a lot of materials to the Qinfang basin during the Silurian-Devonian (e.g., Xu et al., 2017; Zhang et al., 2018). Beyond that, it was previously reported that there are 972 ± 8 Ma Jiangnan rhyolites with ~1100 Ma inherited magmatic zircons exposed in the center of the Cathaysia block (e.g., Shu et al., 2008), 970–890 Ma Shuangxiwu Group volcano-plutonic rocks present on the southeastern margin of the Yangtze block (Li et al., 2009), and Neoproterozoic (900–750 Ma) zircons dominated in the middle-late Neoproterozoic sediments in the Jiangnan orogen (e.g., Wang et al., 2012b, 2012c; Zhao et al., 2011). In combination with the southwestward paleocurrents (Yang et al., 2012), these rocks could serve as another potential source for the Qinfang basin. It is noted that late Neoproterozoic-early Paleozoic (650–500 Ma) detrital zircons occur in samples WG07 with an age peak of 576 Ma and WG08 (Fig. 7). These zircons may have been derived from Cambrian-Silurian sedimentary rocks containing detritus of this age in the Yunkai massif and the basin itself (Xu et al., 2017).

The integration of detrital zircons from the four sandstone samples in this study displays a major age group of Late Cambrian–Early Devonian zircons with ages ranging from 498 to 412 Ma and a corresponding age peak of ~471 Ma that is also present in the age distribution of each sample (Fig. 7), implying that they have a possible common source. This age range corresponds to ~500–410 Ma igneous rocks (e.g., granites) and metamorphic rocks (e.g., gneisses, granulites, migmatites, and amphibolites) that were considered to be produced by the early Paleozoic Kwangsian movement in the SCB (Charvet et al., 2010; Li et al., 2010; Wang et al., 2011a; Xu et al., 2011; Yan et al., 2017). Among them, ~480–410 Ma granitic rocks were extensively exposed in the Yunkai massif (Chen et al., 2012; Peng et al., 2006; Wang et al., 2011b). Also, the age peak of 471 Ma is basically in accordance with the major age peak of 480–460 Ma for Upper Permian-Triassic samples (TWZ4, TWZ65, NSPZ7, and NTZ5) (Hu et al., 2014; Xu et al., 2017) and Devonian and Silurian samples (Xu et al., 2017; Zhang et al., 2018) from the same basin (Figs. 7 and 9) and the Yunkai massif. This fact suggests that the detrital zircons as young as 471 Ma from sandstone clasts within the younger (e.g., Late Permian to Middle Jurassic) strata are in agreement with the source from the older (i.e., early Paleozoic) sediments in the Yunkai massif and the Qinfang basin (e.g., Hu et al., 2014). In combination with the southeast-northwest-directed paleocurrents during Later Permian and Early Triassic in the Shiwandashan area (Fig. 2c; Liang and Li, 2005) and early Paleozoic igneous and sedimentary units in the Yunkai massif (e.g., Chen et al., 2012; Wang et al., 2011b; Yan et al., 2017; Yu et al., 2010; Zhang et al., 2012), the above comparisons imply that detritus of this age were likely derived from the Yunkai massif and its surrounding areas.

Detrital zircon spectra for the Middle Jurassic sample WG06 are distinct from the pre-Triassic material [except for samples ST-7W and ST-9W from the Upper Carboniferous to Permian Bancheng Formation (Ke et al., 2018)] because of both the presence of Middle Carboniferous to Early Triassic (334–246 Ma) detrital grains and the absence of prominent component of Proterozoic grains, but from the Triassic material mainly because of the latter (Figs. 7 and 9). Integration of samples ST-7W and ST-9W displays a similar age distribution to our sample WG06 (Fig. 9a and e), with the youngest detrital zircon age group of 300–265 Ma and the corresponding peak age of ~282 Ma (Fig. 9e; Ke et al., 2018). This age group was considered to most likely source from the Jinshajiang-Ailaoshan-Song Ma-Babu suture belt (Fan et al., 2010; Hennig et al., 2009; Lai et al., 2014; Yan et al., 2006). In addition, Hainan Island (Chen et al., 2011; Li et al., 2002, 2008b; Tang et al., 2013; Xie et al., 2006) and Southeast Yunnan-North Vietnam (Chen et al., 2014; Halpin et al., 2016; Roger et al., 2000) are also the possible source for this age group. As shown in Figs. 4 and 5, the 334–246 Ma detrital zircons are generally subhedral to euhedral, with oscillatory zones and high Th/U ratios (greater than0.1), indicating that the zircons are magmatic in origin and experienced short transportation (e.g., Maas et al., 1992). According to the inference of Hu et al. (2014), Permian-Early Triassic (300–246 Ma) zircons among them are likely supplied by the Darongshan-Shiwandashan granites and dolerites (e.g., Chen et al., 2011; Deng et al., 2004; Xu et al., 2018; Zhao et al, 2010, 2012), which are overlain unconformably by the Upper Triassic strata and immediately close to the Shangsi area where sample WG06 was collected (Fig. 2). Also, zircons of this age may be provided by an older sequence in immediately adjacent Bancheng Town, Qinzhou City where samples ST-7W and ST-9W were collected (Ke et al., 2018). It was recently reported that both one sedimentary rock from the Pingxiang-Chongzuo area (right to the northwest of Qinfang basin) and all the Permian siltstones from Hainan Island are found to contain detrital zircons with a major age group of 400–300 Ma (Hu et al., 2017). Among them, Carboniferous detrital zircons from the Qinfang basin (sample WG06) and the adjacent Pingxiang-Chongzuo area (sample PX20) may be derived from rocks exposed along the southwestern and southeastern margins of the SCB. In terms of Yang et al. (2012) and Hu et al. (2017), for example, the 400–300 Ma ophiolitic gabbros, plagiogranites, and

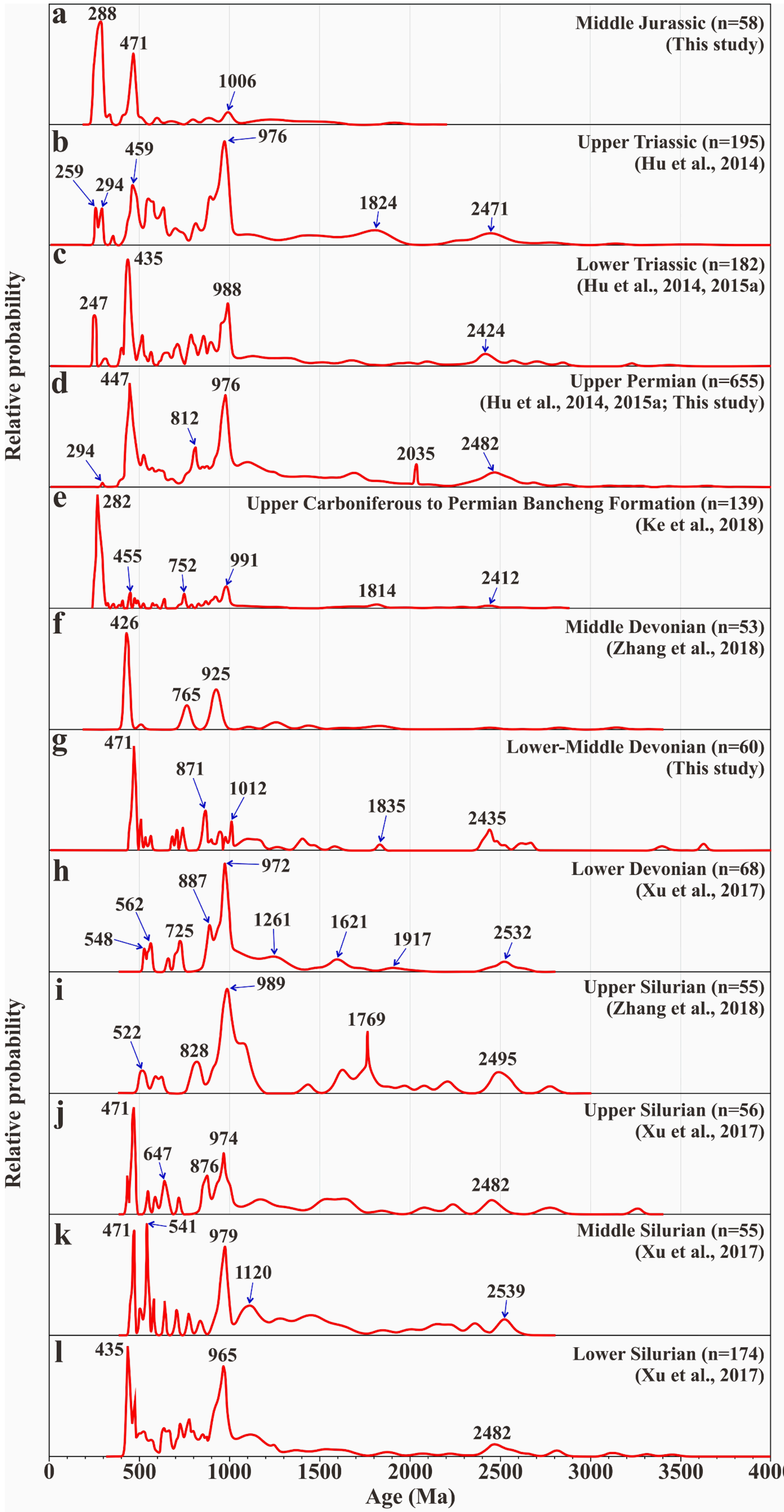

Fig. 9. Relative probability plots comparing U-Pb ages for detrital zircon with rock ages from Lower Silurian to Middle Jurassic in the Qinfang basin (Hu et al., 2014, 2015a; Ke et al., 2018; This study; Xu et al., 2017; Zhang et al., 2018).

tuffs in the Jinshajiang-Ailaoshan-Song Ma-Babu suture zone (Guo et al., 2004; Halpin et al., 2016; Huang, 2013; Jian et al., 2009a, b; Nie et al., 2016; Wu et al., 1999; Zhong et al., 1999; Zi et al., 2012a), associated with the Paleo-Tethys branch ocean, may be responsible for the Devonian-Carboniferous detrital zircons in Lower-Middle Triassic sedimentary rocks in the Youjiang basin and Pingxiang-Chongzuo area, in accord with the northeast-directed paleocurrent data. In turn, Carboniferous (334–300 Ma) zircons in our Middle Jurassic sample, may be derived from such a relatively older sequence in the Youjiang basin and Pingxiang-Chongzuo area, both which and Qinfang basin are considered to form the Greater Youjiang basin, where the Devonian to Triassic strata were deposited (Yang et al., 2012). In contrast, Carboniferous (~330 Ma, He et al., 2018) igneous rocks on Hainan Island are unlikely to feed the Pingxiang-Chongzuo area and Qinfang basin since the Late Permian because the detritus from the Hainan Island cannot pass through a topographic barrier consisting of the Yunkai massif (e.g., Liang and Li, 2005).

6.3. Geological implications

6.3.1. Implications for the affinity of Qinfang basin

Our U-Pb dating of detrital zircons of the sandstones from the Lower-Middle Devonian and Upper Permian sequences in the Qinfang basin both display the youngest age population at ~470 Ma (Fig. 7). This age group is the same as that from the Upper and Middle Silurian sequences (Fig. 9j and k; Xu et al., 2017), younger than that from the Lower Devonian (548 Ma in Fig. 9h; Xu et al., 2017) and Upper Silurian (522 Ma in Fig. 9i; Zhang et al., 2018), and older than that (426–458 Ma) from the Upper Permian (Fig. 10; Hu et al., 2014, 2015a) and Middle Devonian (Fig. 9f; Zhang et al., 2018) and Lower Silurian (435 Ma in Fig. 9l; Xu et al., 2017) sequences. Along the Qinzhou-Fangcheng fault, detrital zircons from the sedimentary rocks in the Upper Permian display a rough consistency but with some changes in the age distribution from the southwest to northeast (Figs. 2 and 10). Furthermore, the age distributions of detrital zircons from the Devonian succession in the basin are distinct between Xu et al. (2017) and Zhang et al. (2018). This is also true for that from the Silurian succession between these two studies. These comparisons suggest either local non-uniformity or insufficient analyses for each sample. It is thus necessary to integrate detrital zircons from sandstones of the same sequence within the basin.

Results show that the youngest age population of detrital zircons from the sandstones in the Qinfang basin is defined at 435 Ma for the Silurian sequence (Fig. 11c; Xu et al., 2017; Zhang et al., 2018), 435 Ma for the Devonian sequence (Fig. 11a; This study; Xu et al., 2017; Zhang et al., 2018), and 447 Ma for the Upper Permian sequence (Hu et al., 2014, 2015a; This study). These ages fall between 460 and 420 Ma during which the Kangsian orogeny occurred, of which crustal thickening took place from 460 to 435 Ma as an early phase, when the amphibolite- to granulite-facies metamorphism, crustal anataxis, and coeval magmatism occurred widely in the Yunkai and Wuyi massifs of the Cathaysia block (Li et al., 2010; Wang et al., 2011a, 2012a; Yu et al., 2005). Ar-Ar dating conducted previously on amphibole and mica in mylonites from the two massifs suggested that after the first stage of compression and thickening, post-orogenic extension and cooling occurred between 435 Ma and 420 Ma (Li et al., 2010; Shu et al., 1999, 2014; Xu et al., 2011, 2016). These facts suggest that the Qinfang basin was likely to form during or after the post-orogenic extension. The similarity in age spectra and Hf isotopic compositions between Silurian samples in the Qinfang basin and those equivalents in both the Ailaoshan belt and Hainan Island suggests that they may be adjacent and fed by a common source during that period (Fig. 11; Xia et al., 2015; Xu et al., 2017; Zhou et al., 2015). At the same time, the Hf isotope data and crustal model ages on zircon grains of early Paleozoic, early Neoproterozoic, and late Mesoproterozoic age groups in our samples WG06 and WG08 are similar to those of zircon grains from Western Australia and Tethyan Himalaya (Fig. 8), both which consisted of a portion of East Gondwana. Furthermore, several studies on the provenance of detritus in the Cambrian-Ordovician strata from the Yunkai massif and west Damingshan (e.g., Wang et al., 2010a; Xu et al., 2013, 2014a), located on the east and west side of the Qinfang basin, respectively, indicated that they also shared a common source. Along with these evidences, the provenance comparisons between the Qinfang basin and its east and west sides (Fig. 12) suggest that the common source they shared in the early Paleozoic is East Gondwana (e.g., Western Australia and Tethyan Himalaya).

6.3.2. Implications for the tectonic setting of Qinfang basin

In the past few decades, many researchers have put forward various views on the tectonic setting of the Qinfang basin during the late Paleozoic: an intracontinental rift (Liu et al., 1993) or a portion of an intracontinental basin (e.g., Yao and Li, 2016), an expanded residual trough (Xu et al., 2001; Zhang and Xia, 1998) or Cambrian ocean (e.g., Li et al., 1994), a passive continental margin (Deng et al., 2003; Zhao et al., 2007), and a part of Paleo-Tethys Ocean (Wu, 1999, 2003; Wu et al., 1994a) or a branch ocean basin of Paleo-Tethys Ocean (He et al., 2018). The Qinfang basin was filled with the Silurian to Middle Devonian siliceous rocks and the overlying Upper Devonian to Upper Permian cherts and silicic mudstones, indicating ongoing regional subsidence (Ma, 1996). Interestingly, synchronous sedimentary evolution also occurred in the Ailaoshan belt (Feng et al., 1999; Xia et al., 2015; Xiong et al., 1998; Xu et al., 2019a; Zhang and Lenz, 1998). This was likely associated with the opening of the Paleo-Tethyan (Ailaoshan) Ocean due to an observation that there are 385–310 Ma mid-ocean ridge basalt (MORB)-type ophiolites exposed along the Jinshajiang-Ailaoshan-SongMa-Hainan Island tectonic belt (e.g., Jian et al., 2009a, 2009b; Zhang et al., 2014). In contrast, there is no ophiolite exposed in the Qinfang basin, and only mudstones interbedded with cherts dominate in the Late Devonian to Carboniferous rock assemblages at the bottom of the basin (e.g., Wang, 1994; Wu et al., 1994b). Also, radiolarians with a Paleo-Tethyan affinity were recognized in the Late Devonian to Late Permian cherts (Ke et al., 2018; Wang, 1994; Wu et al., 1994b), and minor 261 ± 5 Ma island arc-type basalts were found to expose near Yulin area (Zhang et al., 2003). Furthermore, Late Permian to Early Triassic granitic rocks (275–230 Ma), volcanic rocks (e.g., ~250 Ma rhyolites), and mafic rocks (e.g., ~250–248 Ma dolerites) are also widely exposed in the Qinfang basin (Chen et al., 2011; Deng et al., 2004; Xu et al., 2018). These facts suggest that the Qinfang basin is not only a remnant of the Ailaoshan Ocean but also a continental basin rather than an ocean basin. However, Ma (1996) found that a Paleozoic deep-sea deposit appeared in the basin. Recently, Ke et al. (2018) also recognized radiolarian assemblages indicative of a deep-sea or pelagic setting and a Tethyan affinity. Along with the Permian subduction-related arc volcanic rocks and E-MORB type basalts in the Pingxing-Chongzuo area (Qin et al., 2011, 2012), Ke et al. (2018) suggests that the Qinfang basin is a Permian arc-related basin.

In response to the Indosinian orogeny, the basin was once pushed northward over the southern margin of the SCB (e.g., Cai and Zhang, 2009; Zhang and Cai, 2009). As mentioned above, however, detritus of Silurian-Devonian at the bottom of the Qinfang basin were proved to be fed by the immediately adjacent highlands (e.g., the west Damingshan and Yunkai massif). This point, combined with the unconformable relationship between the Silurian-Devonian strata and older strata in the Yunkai massif, suggests that the basin is autochthonous. Different from the inference by Xu et al. (2017) based on only one Devonian sample (including 68 zircon grains), the age distributions of Devonian samples in the Qinfang basin (Fig. 11a; Xu et al., 2017; Zhang et al., 2018; This study) are similar to those of not only equivalents in the Ailaoshan belt (Fig. 11b; Xia et al., 2015), but also Silurian samples in the same basin (Fig. 11c; Xu et al., 2017; Zhang et al., 2018). These similarities show that the Qinfang basin and Ailaoshan belt may be fed by a common source during Silurian to Devonian, supporting that the Qinfang basin is a remnant of the Ailaoshan Ocean. However, they are distinct from those

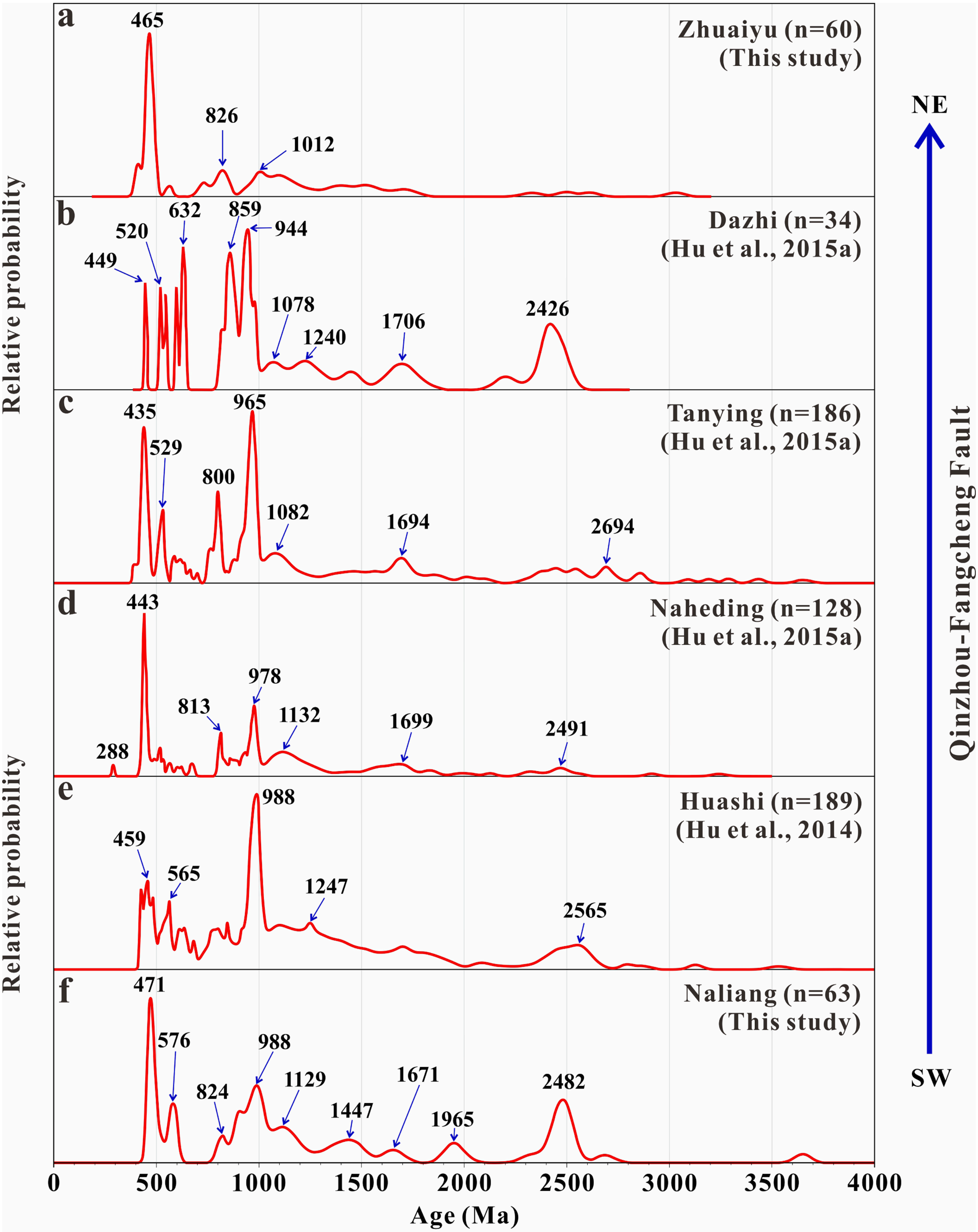

Fig. 10. Relative probability plots comparing U-Pb ages for detrital zircon from Late Permian sandstones along the Qinzhou-Fangcheng Fault (Hu et al., 2014, 2015a; This study).

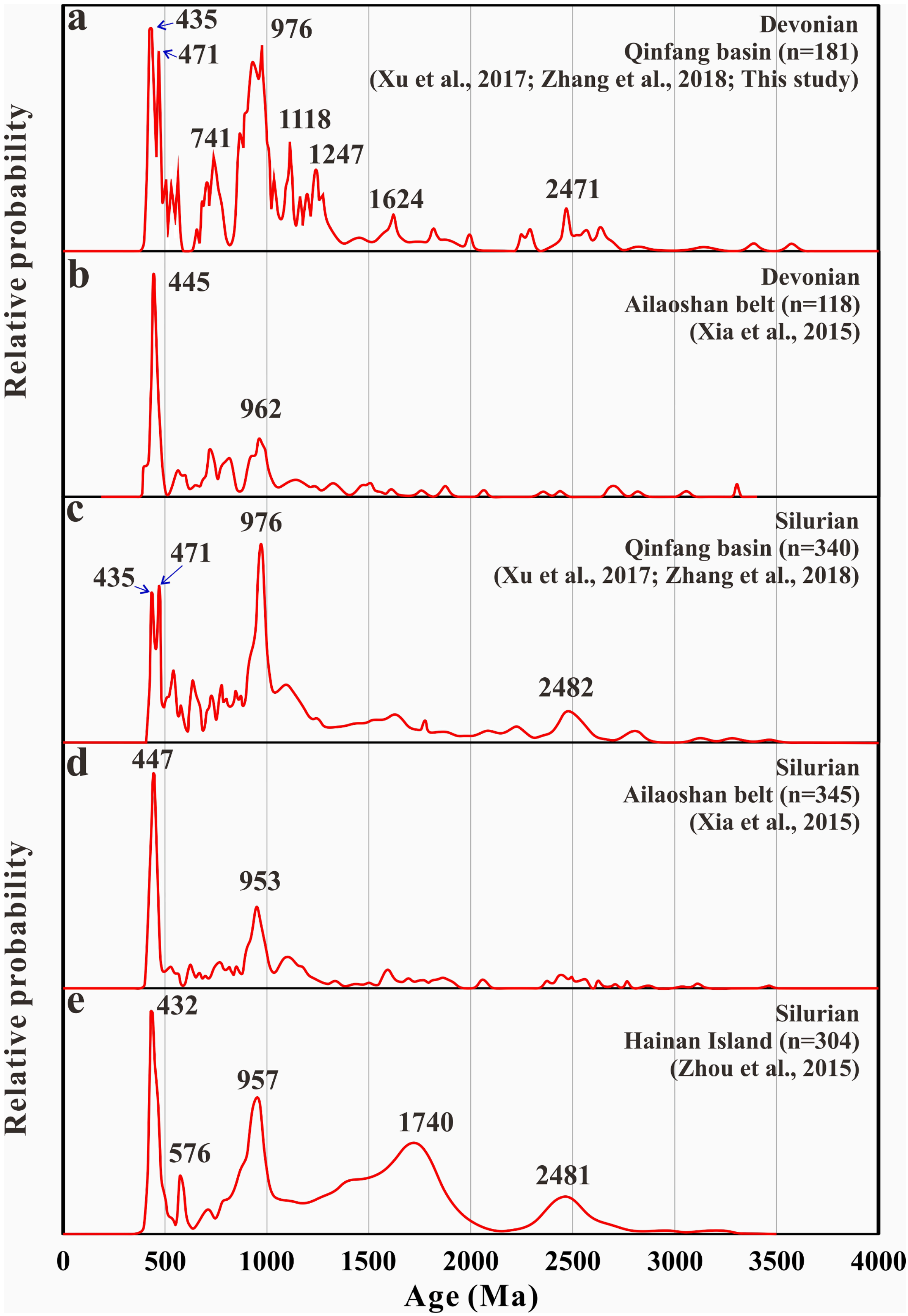

Fig. 11. Age distribution of detrital zircons for Devonian sandstones in the Qinfang basin (Xu et al., 2017; Zhang et al., 2018; This study) and Ailaoshan belt (Xia et al., 2015), and for Silurian sandstones in the Qinfang basin (Xu et al., 2017; Zhang et al., 2018), Ailaoshan belt (Xia et al., 2015), and Hainan Island (Zhou et al., 2015).

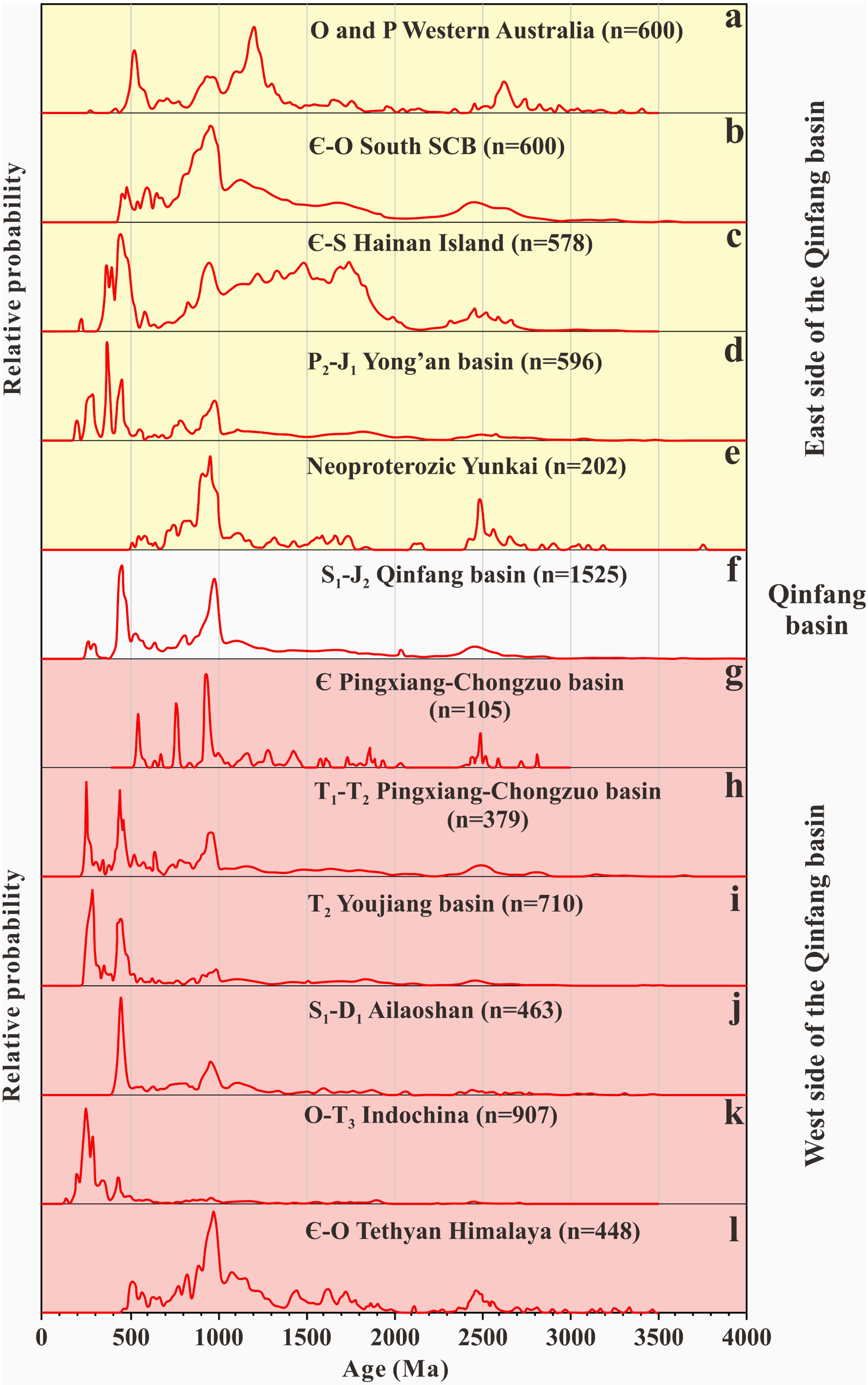
O and P Western Australia (n=600)
a
Є-O South SCB (n=600)
b
Є-S Hainan Island (n=578)
c
P$_2$-J$_1$ Yong'an basin (n=596)
d
Neoproterozic Yunkai (n=202)
e
S$_1$-J$_2$ Qinfang basin (n=1525)
f
Є Pingxiang-Chongzuo basin (n=105)
g
T$_1$-T$_2$ Pingxiang-Chongzuo basin (n=379)
h
T$_2$ Youjiang basin (n=710)
i
S$_1$-D$_1$ Ailaoshan (n=463)
j
O-T$_3$ Indochina (n=907)
k
Є-O Tethyan Himalaya (n=448)
l
Relative probability
Relative probability
East side of the Qinfang basin
Qinfang basin
West side of the Qinfang basin
0
500
1000
1500
2000
2500
3000
3500
4000
Age (Ma)

(caption on next page)

Fig. 12. Relative probability plots comparing U-Pb ages for detrital zircon from the Qinfang basin (Hu et al., 2014, 2015a; Xu et al., 2017; Zhang et al., 2018; This study) and its two sides [east side: O and P Western Australia (Cawood and Nemchin, 2000; Kettanah, 2015; Ksienzyk et al., 2012; Veevers et al., 2005), Є-O South SCB (Chen et al., 2018; Wang et al., 2010b; Xu et al., 2013, 2014a), Є-S Hainan Island (Xu et al., 2014b; Zhou et al., 2015), P_2-J_1 Yong'an basin (Hu et al., 2015b) and Neoproterozic Yunkai (Yu et al., 2008, 2010); west side: Є Pingxiang-Chongzuo basin (Zhang et al., 2018), T_1-T_2 Pingxiang-Chongzuo basin (Hu et al., 2017), T_2 Youjiang basin (Yang et al., 2012), S_1-D_1 Ailaoshan (Xia et al., 2015), O-T_3 Indochina block (Burrett et al., 2014; Yan et al., 2017) and Є-O Tethyan Himalaya (Hughes et al., 2011; Myrow et al., 2010)].

of Ordovician-Upper Triassic samples from the Indochina block (Fig. 12k; Burrett et al., 2014; Yan et al., 2017), indicating that the Qinfang basin is not a part of the Indochina block.

Similar to the Qinfang basin, the Late Devonian cherts in the adjacent Youjiang basin also contain radiolarians characterized by a Paleo-Tethyan affinity (e.g., Ren et al., 2011) and the basin was also formed in association with the Ailaoshan Ocean opening (Du et al., 2013; Guo et al., 2004; Huang et al., 2013). These evidences suggest that both the two basins were linked during this period. Until the Late Carboniferous to Early Permian, the Qinfang-Pingxiang-Chongzuo-Youjiang (i.e., Greater Youjiang) basin reached a maximum area, where voluminous interbedding of banded black cherts and thin mudstones accumulated. However, this is distinct from the overlying Middle Permian stratum that is characterized by the interbedding of thin mudstones and thin cherts, which in turn have an unconformable contact with their overlying siliciclastic turbidites of Late Permian (Huang et al., 2013; Qiu et al., 2017). Previous studies suggested that the change in these facies was synchronous with the transition of the Ailaoshan Ocean from divergence to convergence (e.g., Jian et al., 2009b; Zi et al., 2012b).

The Ailaoshan Ocean was generally inferred to close at ~260–220 Ma (e.g., Lai et al., 2014). However, two recent studies by Xu et al. (2019a, 2019b) suggested that the final closure of the Ailaoshan Ocean occurred in the Late Triassic. The subsequent oblique collision between the SCB and Indochina block occurred in the period of Late Permian-Middle Triassic (Faure et al., 2016; Liu et al., 2015; Zi et al., 2013), resulting in the shallowing of carbonate sediment from marine to terrestrial, which is inferred to mark a conversion to a foreland basin from an intracontinental basin (e.g., Cai and Zhang, 2009; Faure et al., 2016; Zhao et al., 2012). This process is exactly the Indosinian orogeny that led to diachronous convergence of the Great Youjiang basin (Hu et al., 2015a; Zhao et al., 2012), from the Late Permian convergence in the Qinfang area, through the Early Triassic convergence in the Pingxiang-Chongzuo area, and finally to the Middle Triassic convergence in the Youjiang area (Hu et al., 2014, 2015b, 2017; Liang and Li, 2005; Qiu et al., 2017; Yang et al., 2013). This means that the Greater Youjiang basin experienced a transition to a contraction-related foreland basin from an extension-related continental rift-to-drift basin during the Indosinian event (e.g., Hu et al., 2017). Also, it induced crustal thickening and uplift of the basin due to both collision and input of voluminous siliciclastic turbidites from the immediately highland (Liang and Li, 2005; Hu et al., 2014; Xing et al., 2016; Yang et al., 2012). By the Middle Jurassic, however, the Qinfang basin has received much more Middle Carboniferous- Early Triassic detrital zircons from the relatively older strata in the western immediately area (e.g., T_1-T_2 Pingxiang-Chongzuo basin and T_2 Youjiang basin; Figs. 9 and 12) or basin self (Fig. 9e), but not from the east side of the Qinfang basin (e.g., P_2-J_1 Yong'an basin; Fig. 12) because the subhedral to euhedral zircon crystals, indicative of short transportation from their source region, were found in the Middle Jurassic sample (Fig. 4a). This suggests that the adjacent west side of the Qinfang basin may be still tectonically active at least until the Middle Jurassic.

7. Conclusions

Lower-Middle Devonian to Middle Jurassic sandstones exhibit an overall age distribution pattern of detrital zircon characterized by major age groups at 2700–2300 Ma (absence for Jurassic), 1200–800 Ma, 600–400 Ma, and 334–246 Ma (for Jurassic alone). Zircons (peak ~2500 Ma) was derived from the Yangtze block, while ~1200–800 Ma grains may be sourced from the Yunkai massif and Jiangnan orogen. Zircons of ~600–400 Ma came from Yunkai massif and/or recycled from Cambrian to Silurian sediments of the basin itself. Carboniferous-Early Triassic (334–246 Ma) zircons were likely to be supplied by an older sequence in the Great Youjiang basin and the Darongshan-Shiwandashan igneous rocks. The Qinfang basin and its two sides are considered to share a common East Gondwana source in the period of Silurian. The similarity in age spectra between Silurian-Devonian samples in the basin and the Ailaoshan belt suggests that the basin is a remnant of the Paleo-Tethyan (Ailaoshan) Ocean. However, the distinct age distribution between the Qinfang basin and Indochina block shows that the basin is not a part of the Indochina block. By Middle Jurassic following the final closure of the Ailaoshan Ocean in the Late Triassic, the adjacent western area may be still tectonically active, thereby feeding the basin with detritus of Early Permian.

CRediT authorship contribution statement

Tongbin Shao: Conceptualization, Writing - original draft, Writing - review & editing. **Yun Zhou:** Data curation, Methodology, Writing - review & editing. **Yongfeng Cai:** Writing - review & editing, Funding acquisition. **Xinquan Liang:** Data curation, Methodology, Investigation. **Maoshuang Song:** Investigation, Funding acquisition.

Declaration of Competing Interest

The authors declare that they have no known competing financial interests or personal relationships that could have appeared to influence the work reported in this paper.

Acknowledgments

We appreciate the critical and constructive comments of Dr. Jianwei Zi and an anonymous reviewer and the Editor Prof. Michel Faure that helped us to improve the manuscript. This work was supported by the Guangxi Natural Science Foundation Program (Nos. 2015GXNSFBA139204 and 2017GXNSFAA198209), the Strategic Priority Research Program (B) of the Chinese Academy of Sciences (No. XDB18010402), the Pearl River Talent Plan of Guangdong Province, and the research grant of SKLIG (No. SKLabIG–KF–16–06). This is a contribution to No. IS-2922 from GIGCAS.

Appendix A. Supplementary material

Supplementary data to this article can be found online at https://doi.org/10.1016/j.jseaes.2020.104578.

References

Arboit, F., Collins, A.S., King, R., Morley, C.K., Hansberry, R., 2014. Structure of the Sibumasu-Indochina collision, central Thailand: A section through the Khao Khwang fold and thrust belt. J. Asian Earth Sci. 95, 182–191.

Belousova, E.A., Kostitsyn, Y.A., Begg, G.C., Griffin, W.L., O'Reilly, S.Y., Pearson, N.J., 2010. The growth of the continental crust: constraints from zircon Hf-isotope data. Lithos 119, 457–466.
BGMRGP (Bureau of Geology and Mineral Resources of Guangdong Province), 1988. Regional geology of the Guangdong Province. Beijing, Geological Publishing House, 941p (in Chinese with English abstract).
BGMRGZAR (Bureau of Geology and Mineral Resources of Guangxi Zhuang Autonomous Region), 1985. Regional geology of the Guangxi Zhuang Autonomous Region. Beijing, Geological Publishing House, 853p (in Chinese with English abstract).
Blichert, T.J., Chauvel, C., Albarede, F., 1997. Separation of Hf and Lu for high-precision isotope analysis of rock samples by magnetic sectormultiple collector ICP-MS. Contrib. Miner. Petrol. 127 (3), 248–260.
Burrett, C., Zaw, K., Meffre, S., Lai, C.K., Khositanont, S., Chaodumrong, P., Udchachon, M., Ekins, S., Halpin, J., 2014. The configuration of Greater Gondwana - Evidence from LAICPMS, U-Pb geochronology of detrital zircons from the Palaeozoic and Mesozoic of Southeast Asia and China. Gondwana Res. 26 (1), 31–51.
Cai, J.X., Zhang, K.J., 2009. A new model for the Indochina and South China collision during the late Permian to the middle Triassic. Tectonophysics 467, 35–43.
Carter, A., Roques, D., Bristow, C., Kinny, P., 2001. Understanding Mesozoic accretion in Southeast Asia: significance of Triassic thermotectonism (Indosinian orogeny) in Vietnam. Geology 29 (3), 211–214.
Cawood, P.A., Nemchin, A.A., 2000. Provenance record of a rift basin: U/Pb ages of detrital zircons from the Perth Basin, Western Australia. Sediment. Geol. 134, 209–234.
Cawood, P.A., Wang, Y.J., Xu, Y.J., Zhao, G.C., 2013. Locating South China in Rodinia and Gondwana: A fragment of Greater India Lithosphere? Geology 41, 903–906.
Cawood, P.A., Wang, W., Zhao, T., Xu, Y., Mulder, J.A., Pisarevsky, S.A., Zhang, L., Gan, C., He, H., Liu, H., Qi, L., Wang, Y., Yao, J., Zhao, G., Zhou, M.-F., Zi, J.-W., 2020. Deconstructing South China and consequences for reconstructing Nuna and Rodinia. Earth Sci. Rev. 204 https://doi.org/10.1016/j.earscirev.2020.103169.
Cawood, P.A., Zhao, G.C., Yao, J.L., Wang, W., Xu, Y.J., Wang, Y.J., 2018. Reconstructing South China in Phanerozoic and Precambrian supercontinents. Earth-Sci. Rev. 186, 173–194.
Charvet, J., 2013. The Neoproterozoic-early Paleozoic tectonic evolution of the South China Block: An overview. J. Asian Earth Sci. 74, 198–209.
Charvet, J., Shu, L.S., Faure, M., Wang, B., Lu, H.F., Breton, N.L., 2010. Structural development of the lower Paleozoic belt of South China: Genesis of an intracontinental orogeny. J. Asian Earth Sci. 39, 309–330.
Chen, C.H., Hsieh, P.S., Lee, C.Y., Zhou, H.W., 2011. Two episodes of the Indosinian thermal event on the South China Block: constraints from LA-ICPMS U-Pb zircon and electron microprobe monazite ages of the Darongshan S-type granitic suite. Gondwana Res. 19, 1008–1023.
Chen, Z., Lin, W., Faure, M., Lepvrier, C., Van Vuong, N., Van Tich, V., 2014. Geochronology and isotope analysis of the Late Paleozoic to Mesozoic granitoids from northeastern Vietnam and implications for the evolution of the South China block. J. Asian Earth Sci. 86, 131–150.
Chen, C.H., Liu, Y.H., Lee, C.Y., Xiang, H., Zhou, H.W., 2012. Geochronology of granulite, charnockite and gneiss in the poly-metamorphosed Gaozhou Complex (Yunkai Massif), South China: emphasis on the in-situ EMP monazite dating. Lithos 144–145, 109–129.
Chen, Q., Sun, M., Long, X., Zhao, G., Wang, J., Yu, Y., Yuan, C., 2018. Provenance study for the Paleozoic sedimentary rocks from the west Yangtze Block: constraint on possible link of South China to the Gondwana supercontinent reconstruction. Precambr. Res. 309, 271–289.
Deng, X.G., Chen, Z.Q., Li, X.H., Liu, D.Y., 2004. SHRIMP U-Pb zircon dating of the Darongshan-Shiwandashan granitoid belt in southeastern Guangxi, China. Geol. Rev. 50, 426–442 (in Chinese with English abstract).
Deng, X.G., Li, X.H., Chen, Z.G., 2003. Geochemical features and sedimentary setting of Late Devonian cherts in Bancheng of Qinzhou, Guangxi. Chin. J. Geol. 38, 460–469 (in Chinese with English abstract).
Dong, S.W., Zhang, Y.Q., Gao, R., Su, J.B., Liu, M., Li, J.H., 2015. A possible buried Paleoproterozoic collisional orogeny beneath central South China: Evidence from seismic-reflection profiling. Precambr. Res. 264, 1–10.
Dong, Y.P., Zhang, G.W., Neubauer, F., Liu, X.M., Genser, J., Hauzenberger, C., 2011. Tectonic evolution of the Qinling orogeny, China: a review and synthesis. J. Asian Earth Sci. 41, 213–237.
Du, Y.S., Huang, H., Yang, J.H., Huang, H.W., Tao, P., Huang, Z.Q., Hu, L.S., Xie, C.X., 2013. The basin translation from Late Paleozoic to Triassic of the Youjiang Basin and its tectonic signification. Geol. Rev. 59 (1), 1–11 (in Chinese with English abstract).
Fan, W.M., Wang, Y.J., Zhang, A.M., et al., 2010. Permian arc-back-arc basin development along the Ailaoshan tectonic zone: geochemical isotopic and geochronological evidence from the Mojiang volcanic rocks, southwest China. Lithos 119 (3–4), 553–568.
Faure, M., Lepvrier, C., Nguyen, V.V., Vu, V.T., Lin, W., Chen, Z., 2014. The South China block-Indochina collision: Where, when, and how? J. Asian Earth Sci. 79, 260–274.
Faure, M., Lin, W., Chu, Y., Lepvrie, C., 2016. Triassic tectonics of the Ailaoshan Belt (SW China): Early Triassic collision between the South China and Indochina Blocks, and Middle Triassic intracontinental shearing. Tectonophysics 683, 27–42.
Faure, M., Shu, L.S., Wang, B., Charvet, J., Choulet, F., Monie, P., 2009. Intracontinental subduction: A possible mechanism for the Early Palaeozoic Orogen of SE China. Terra Nova 21, 360–368.
Feng, Q.L., Ge, M.C., Xie, D.F., Ma, Z.D., Jiang, Y.S., 1999. Stratigraphic sequence and tectonic evolution in passive continental margin, Jinshajiang Belt, northwestern Yunnan, China. J. China Univ. Geosci. 24 (6), 553–557 (in Chinese with English abstract).
Griffin, W.L., Pearson, N., Belousova, E., Jackson, S., Achterbergh, E.V., O'Reilly, S.Y., Shee, S., 2000. The Hf isotope composition of cratonic mantle: LAM-MC-ICPMS analysis of zircon megacrysts in kimberlites. Geochim. Cosmochim. Acta 64, 133–147.
Griffin, W.L., Wang, X., Jackson, S., Pearson, S., O'Reilly, S.Y., Xu, X., Zhou, X., 2002. Zircon chemistry and magma mixing, SE China: In-situ analysis of Hf isotopes, Tonglu and Pingtan igneous complexes. Lithos 61 (3–4), 237–269.
Guo, F., Fan, W.M., Wang, Y.J., Li, C.W., 2004. Upper Paleozoic basalts in the Southern Yangtze Block: geochemical and Sr-Nd isotopic evidence for asthenosphere-lithosphere interaction and opening of the Paleo-Tethyan Ocean. Int. Geol. Rev. 46 (4), 332–346.
Hacker, B.R., Ratschbacher, L., Webb, L., Ireland, T., Walker, D., Dong, S.W., 1998. U-Pb zircon ages constrain the architecture of the ultrahigh-pressure Qinling-Dabie Orogen, China. Earth Planet. Sci. Lett. 161, 215–230.
Halpin, J.A., Tran, H.T., Lai, C.K., Meffre, S., Crawford, A.J., Zaw, K., 2016. U-Pb zircon geochronology and geochemistry from NE Vietnam: a 'tectonically disputed' territory between the Indochina and South China blocks. Gondwana Res. 34, 254–273.
He, W.H., Xiao, Y.F., Ke, X., Zhang, Z.Y., Yao, H.Z., 2018. The Qinfang basin is a branch of the Paleo-Tehys Ocean: evidence from paleontology and sedimentology. The Twelfth National Congress of the Chinese Society of Paleontology and the 29th Annual Academic Conference.
Hidaka, H., Shimizu, H., Adachi, M., 2002. U-Pb geochronology and REE geochemistry of zircons from Palaeoproterozoic paragneiss clasts in the Mesozoic Kamiaso conglomerate, central Japan: evidence for an Archean provenance. Chem. Geol. 187, 279–293.
Hu, L.S., Cawood, P.A., Du, Y.S., Xu, Y.J., Xu, W.C., Huang, H.W., 2015a. Detrital records for Upper Permian-Lower Triassic succession in the Shiwandashan Basin, South China and implication for Permo-Triassic (Indosinian) orogeny. J. Asian Earth Sci. 98, 152–166.
Hu, L.S., Cawood, P.A., Du, Y.S., Xu, Y.J., Wang, C.H., Wang, Z.W., Ma, Q.L., Xu, X.R., 2017. Permo-Triassic detrital records of South China and implications for the Indosinian events in East Asia. Palaeogeogr. Palaeoclimatol. Palaeoecol. 485, 84–100.
Hu, L.S., Cawood, P.A., Du, Y.S., Yang, J.H., Jiao, L.X., 2015b. Late Paleozoic to Early Mesozoic provenance record of Paleo-Pacific subduction beneath South China. Tectonics 34, 986–1008.
Hu, L.S., Du, Y.S., Cawood, P.A., Xu, Y.J., Yu, W.C., Zhu, Y.H., Yang, J.H., 2014. Drivers for late Paleozoic to early Mesozoic orogenesis in South China: Constraints from the sedimentary record. Tectonophysics 618, 107–120.
Huang, H., 2013. The Basin Translation from the Late Paleozoic to Middle Triassic of the Youjiang Basin-Evidence from Geochemistry of Sedimentary and Volcanic Rocks. China University of Geoscience (Wuhan), Ph.D. thesis, pp.1–160 (in Chinese with English abstract).
Huang, H., Du, Y.S., Huang, Z.Q., Yang, J.H., Huang, H.W., Xie, C.X., Hu, L.S., 2013. Depositional chemistry of chert during late Paleozoic from western Guangxi and its implication for the tectonic evolution of the Youjiang Basin. Sci. China Earth Sci. 56, 479–493.
Hughes, N.C., Myrow, P.M., McKenzie, N.R., Harper, D.A.T., Bhargava, O.N., Tangri, S. K., Ghalley, K.S., Fanning, C.M., 2011. Cambrian rocks and faunas of the Wachi La, Black Mountains, Bhutan. Geol. Magaz. 148 (3), 351–379.
Jian, P., Liu, D., Kroner, A., Zhang, Q., Wang, Y., Sun, X., Zhang, W., 2009a. Devonian to Permian plate tectonic cycle of the Paleo-Tethys Orogen in southwest China (I): geochemistry of ophiolites, arc/back-arc assemblages and within-plate igneous rocks. Lithos 113 (3), 748–766.
Jian, P., Liu, D., Kroner, A., Zhang, Q., Wang, Y., Sun, X., Zhang, W., 2009b. Devonian to Permian plate tectonic cycle of the Paleo-Tethys Orogen in southwest China (II): insights from zircon ages of ophiolites, arc/back-arc assemblages and within-plate igneous rocks and generation of the Emeishan CFB province. Lithos 113 (3), 767–784.
Ke, X., Zhang, Z.Y., Yang, J.H., Yao, H.Z., Zhu, L.K., He, W.H., 2018. Radiolarian and detrital zircon in the Upper Carboniferous to Permian Bancheng Formation, Qinfang basin, and the geological significance. J. Earth Sci. 29 (3), 594–606.
Kettanah, Y.A., 2015. Provenance of the Ordovician-lower Silurian Tumblagooda Sandstone, Western Australia. Aust. J. Earth Sci. 62 (7), 817–830.
Kinny, P.D., Wijbrans, J.R., Froude, D.O., Williams, I.S., Compston, W., 1990. Age constraints on the geological evolution of the Narryer gneiss complex, western Australia. Aust. J. Earth Sci. 37, 51–69.
Ksienzyk, A.K., Jacobs, J., Boger, S.D., Kosler, J., Sircombe, K.N., Whitehouse, M.J., 2012. U-Pb ages of metamorphic monazite and detrital zircon from the Northampton Complex: evidence of two orogenic cycles in Western Australia. Precambr. Res. 198–199, 37–50.
Lai, C.K., Meffre, S., Crawford, A.J., et al., 2014. The central Ailaoshan ophiolite and modern analogs. Gondwana Res. 26 (1), 75–88.
Lepvrier, C., Vuong, N.V., Maluski, H., Thi, P.T., Vu, T.V., 2008. Indosinian tectonics in Vietnam. C.R. Geoscience 340, 94–111.
Li, J.H., Dong, S.W., Zhang, Y.Q., Zhao, G.C., Johnston, S.T., Sun, H.S., Xin, Y.J., 2016. New insights into Phanerozoic tectonics of South China: Part 1, polyphaser deformation in the central Jiangnan Orogen. J. Geophys. Res. 121, 3048–3080.
Li, X.Q., Liu, W.J., Zheng, R.C., 1994. Formation of Qinzhou-Fangcheng folding belt and its geological influence. Guangxi Geol. 7, 15–25 (in Chinese with English abstract).
Li, X.H., Li, W.X., Li, Z.X., Lo, C.H., Wang, J., Ye, M.F., Yang, Y.H., 2009. Amalgamation between the Yangtze and Cathaysia Blocks in South China: Constraints from SHRIMP U-Pb zircon ages, geochemistry and Nd-Hf isotopes of the Shuangxiwu volcanic rocks. Precambr. Res. 174 (1–2), 117–128.

Li, X.H., Li, Z.X., Ge, W.C., Zhou, H.W., Li, W.X., Liu, Y., Wingate, W.T.D., 2003. Neoproterozoic granitoids in South China: Crustal melting above a mantle plume at ca 825 Ma? Precambr. Res. 122, 45–83.
Li, X.H., Li, Z.X., He, B., Li, W.X., Li, Q.L., Gao, Y., Wang, X.C., 2012. The Early Permian active continental margin and crustal growth of the Cathaysia Blocks: in situ U-Pb, Lu-Hf and O isotope analyses of detrital zircons. Chem. Geol. 328, 195–207.
Li, Z.X., Li, X.H., 2007. Formation of the 1300-km-wide intracontinental orogeny and postorogenic magmatic province in Mesozoic South China: a flat-slab subduction model. Geology 35 (2), 179–182.
Li, W.X., Li, X.H., Li, Z.X., Lou, F.S., 2008a. Obduction-type granites within the NE Jiangxi Ophiolite: implications for the final amalgamation between the Yangtze and Cathaysia Blocks. Gondwana Res. 13, 288–301.
Li, Z.X., Li, X.H., Wartho, J.A., Clark, C., Li, W.X., Zhang, C.L., Bao, C.M., 2010. Magmatic and metamorphic events during the early Paleozoic Wuyi-Yunkai orogeny, southeastern South China: new age constraints and pressure-temperature conditions. Geol. Soc. Am. Bull. 122 (5–6), 772–793.
Li, Z.X., Li, X.H., Zhou, H.W., Kinny, P.D., 2002. Grenvillian continental collision in South China: New SHRIMP U-Pb zircon results and implications for the configuration of Rodinia. Geology 30, 163–166.
Li, Z.X., Li, X.H., Li, W.X., Ding, S.J., 2008b. Was Cathaysia part of Proterozoic Laurentia?-New data from Hainan Island, South China. Terra Nova 20 (2), 154–164.
Li, Z.X., Wartho, J.A., Occhipinti, S., Zhang, C.L., Li, X.H., Wang, J., Bao, C., 2007. Early history of the eastern Sibao Orogen (South China) during the assembly of Rodinia: New mica 40Ar/39Ar dating and SHRIMP U-Pb detrital zircon provenance constraints. Precambr. Res. 159, 79–94.
Liang, X.Q., Li, X.H., 2005. Late Permian to Middle Triassic sedimentary records in Shiwandashan basin: Implication for the Indosinian Yunkai orogenic belt, South China. Sed. Geol. 177, 297–320.
Lin, W., Wang, Q., Chen, K., 2008. Phanerozoic tectonic of South China Block: New insights from the polyphaser deformation in the Yunkai massif. Tectonics 27, TC6004. https://doi.org/10.1029/2007TC002207.
Liu, Y.S., Gao, S., Hu, Z., Gao, C., Zong, K., Wang, D., 2010. Continental and oceanic crust recycling-induced melt-peridotite interactions in the Trans-North China Orogen: U-Pb dating Hf isotopes and trace elements in zircons from mantle xenoliths. J. Petrol. 51, 537–571.
Liu, Y.S., Hu, Z.C., Gao, S., Gunther, D., Xu, J., Gao, C.G., Chen, H.H., 2008. In situ analysis of major and trace elements of anhydrous minerals by LA-ICP-MS without applying an internal standard. Chem. Geol. 257, 34–43.
Liu, B.J., Xu, X.S., 1994. Atlas of lithofacies and paleogeography of South China. Science Press, Beijing (in Chinese with English abstract).
Liu, B.J., Xu, X.S., Pan, X.N., et al., 1993. Paleocontinent Deposits, Crust Revolution and Mineralization in Southern China. China Science Publishing & Media Ltd., Beijing (in Chinese).
Liu, H.C., Wang, Y.J., Cawood, P.A., Fan, W.M., Cai, Y.F., Xing, X.W., 2015. Record of Tethyan Ocean closure and Indosinian collision along the Ailaoshan suture zone (SW China). Gondwana Res. 27, 1292–1306.
Ludwig, K.R., 2001. Users manual for Isoplot/Ex rev.2.49. Berkeley Geochronology Centre Special. Publication (No. 1a) 1–56.
Ma, W.P., 1996. Paleothys in South China, Permian Orogeny and the Eastwards Extension of Interchange Domain. Scientia Geologica Sinica 31 (2), 105–113 (in Chinese with English abstract).
Maas, R., Kinny, P.D., Williams, I.S., Froude, D.O., Compston, W., 1992. The earth oldest known crust: a geochronological and geochemical study of 3900–4200 Ma old detrital zircons from Mt Narryer and Jack Hills, western-Australia. Geochim. Cosmochim. Acta 56, 1281–1300.
Meng, Q.R., Zhang, G.W., 2000. Geologic framework and tectonic evolution of the Qinling orogeny, central China. Tectonophysics 323, 183–196.
Metcalfe, I., 2006. Palaeozoic and Mesozoic tectonic evolution and palaeogeography of East Asian crustal fragments: the Korean Peninsula in context. Gondwana Res. 9, 24–46.
Metcalfe, I., 2013. Gondwana dispersion and Asian accretion: tectonic and palaeogeographic evolution of eastern Tethys. J. Asian Earth Sci. 66, 1–33.
Myrow, P.M., Hughes, N.C., Goodge, J.W., Fanning, C.M., Williams, I.S., Peng, S., Bhargava, O.N., Parcha, S.K., Pogue, K.R., 2010. Extraordinary transport and mixing of sediment across Himalayan central Gondwana during the Cambrian-Ordovician. Geol. Soc. Am. Bull. 122 (-10), 1660–1670.
Nie, X., Feng, Q., Metcalfe, I., Baxter, A.T., Liu, G., 2016. Discovery of a Late Devonian magmatic arc in the southern Lancangjiang zone, western Yunnan: geochemical and zircon U-Pb geochronological constraints on the evolution of Tethyan ocean basins in SW China. J. Asian Earth Sci. 118, 32–50.
Peng, S.B., Jin, Z.M., Liu, Y.H., Fu, J.M., He, L.Q., Cai, M.H., Wang, Y.B., 2006. Petrochemistry, chronology and tectonic setting of strong peraluminous anatectic granitoids in Yunkai Orogenic Belt, western Guangdong Province, China. J. China Univ. Geosci. 17, 1–12.
Peng, S.B., Liu, S.F., Lin, M.S., Wu, C.F., Han, Q.S., 2016a. Early Paleozoic subduction Cathaysia (I): New evidence from Nuodong ophiolite. Earth Sci. 41, 765–778 (in Chinese with English abstract).
Peng, S.B., Liu, S.F., Lin, M.S., Wu, C.F., Han, Q.S., 2016b. Early Paleozoic subduction Cathaysia (II): New evidence from the Dashuang high magnesian-magnesian andesite. Earth Sci. 41, 931–947 (in Chinese with English abstract).
Peng, M., Wu, Y.B., Wang, J., Jiao, W.F., Liu, X.C., Yang, S.H., 2009. Paleoproterozoic mafic dyke from kongling terrain in the Yangtze Craton and its implication. Chin. Sci. Bull. 54, 1098–1104.
Qin, X.F., Pan, Y.M., Li, R.S., Zhou, F.S., Hu, G.A., Zhong, F., 2006. Zircon SHRIMP U-Pb geochronology of the Yunkai metamorphic complex in southeastern Guangxi. China. Geol. Bull. China 25, 553–559 (in Chinese with English abstract).
Qin, X.F., Wang, Z.Q., Zhang, Y.L., et al., 2011. Geochronology and geochemistry of Early Mesozoic acid volcanic rocks from southwest Guangxi: constraints on tectonic evolution of the southwest segment of Qinzhou-Hangzhou joint belt. Acta Petrologica Sinica 27 (3), 794–808 (in Chinese with English abstract).
Qin, X.F., Wang, Z.Q., Zhang, Y.L., et al., 2012. Geochemistry of Permian mafic igneous rocks from the Napo-Qinzhou tectonic belt in southwest Guangxi, southwest China: Implications for arc-back arc basin magmatic evolution. Acta Geologica Sinica – English Edition 86 (5), 1182–1199.
Qiu, Y.M., Gao, S., Mcnaughton, N.J., Groves, D.L., Ling, W.L., 2000. First evidence of >3.2 Ga continental crust in the Yangtze craton of South China and its implications for Archean crustal evolution and Phanerozoic tectonics. Geology 28 (1), 11–14.
Qiu, L., Yan, D.P., Yang, W.X., Wang, J.B., Tang, X.L., Ariser, S., 2017. Early to Middle Triassic sedimentary records in the Youjiang basin, South China: Implications for Indosinian orogenesis. J. Asian Earth Sci. 141, 125–139.
Ren, J.S., Li, C., 2016. Cathaysia old land and relevant problems: Pre-Devonian tectonics of South China. Acta Geol. Sin. 90, 607–614 (in Chinese with English abstract).
Ren, G.M., Wang, P., Zhang, L., Zhang, B., Dai, J., 2011. Discussion on geochemical characteristics and sedimentary environment of the Frasnian radiolarian chert in southeastern Yunnan. Geol. Rev. 57, 505–514.
Roger, F., Leloup, P.H., Jolivet, M., Lacassin, R., Trinh, P.T., Brunel, M., Seward, D., 2000. Long and complex thermal history of the Song Chay metamorphic dome (northern Vietnam) by multi-system geochronology. Tectonophysics 321, 449–466.
Scherer, E., Munker, C., Mezger, K., 2001. Calibration of the lutetium-hafnium clock. Science 239 (5530), 683–687.
Shu, L.S., Faure, M., Yu, J.H., Jahn, B.M., 2011. Geochronological and geochemical features of the Cathaysia block (South China): new evidence for the Neoproterozoic breakup of Rodinia. Precambr. Res. 187, 263–276.
Shu, L.S., Jahn, B.M., Charvet, J., Santosh, M., Wang, B., Xu, X.S., Jiang, S.Y., 2014. Intraplate tectono-magmatism in the Cathaysia Block (South China): Evidence from stratigraphic, structural, geochemical and geochronological investigations. Am. J. Sci. 314, 154–186.
Shu, L.S., Lu, H.F., Jia, D., Charvet, J., Faure, M., 1999. Study of the 40Ar/39Ar isotopic age for the early Paleozoic tectonothermal event in the Wuyishan region, South China. J. Nanjing Univ. Nat. Sci. 35 (6), 668–674.
Shu, L.S., Wang, B., Cawood, P.A., Santosh, M., Xu, Z.Q., 2015. Early Paleozoic and early Mesozoic intraplate tectonic and magmatic events in the Cathaysia block, South China. Tectonics 34, 1600–1621.
Shu, L.S., Yu, J.H., Jia, D., Wang, B., Shen, W., Zhang, Y.Q., 2008. Early Paleozoic orogenic belt in the eastern segment of South China (in Chinese with English abstract). Geological Bulletin of China 27, 1581–1593.
Tang, L.M., Chen, H.L., Dong, W.C., Yang, S.F., Shen, Z.Y., Chen, X.G., Fu, L.L., 2013. Middle Triassic post-orogenic extension on Hainan Island: chronology and geochemistry constraints of bimodal intrusive rocks. Science China Earth Sciences 56, 783–793.
Ting, W.K., 1929. The orogenic movement in China. Bull. Geol. Soc. China 8, 151–170.
Veevers, J.J., Saeed, A., Belousova, E.A., Griffin, W.L., 2005. U-Pb ages and source composition by Hf-isotope and trace-element analysis of detrital zircons in Permian sandstone and modem sand from southwestern Australia and a review of the paleogeographical and denudational history of the Yilgam craton. Earth Sci. Rev. 68, 245–279.
Vervoort, J.D., Blichert, T.J., 1999. Evolution of the depleted mantle: Hf isotope evidence from juvenile rocks through time. Geochim. Cosmochim. Acta 63 (3–4), 533–556.
Vuong, V.N., Hansen, B.T., Wemmer, K., Lepvrier, C., Tich, V.V., Thang, T.T., 2013. U-Pb and Sm/Nd dating on ophiolitic rocks of the Song Ma suture zone (northern Vietnam): evidence for upper Paleozoic paleotethyan lithospheric remnants. J. Geodyn. 69, 140–147.
Wan, T.F., 2010. The tectonics of China. Springer, Heidelberg, High Education Press, Beijing, p. 501.
Wang, L.J., Yu, J.H., Griffin, W., O'Reilly, S., 2011a. Early crustal evolution in the western Yangtze Block: evidence from U-Pb and Lu-Hf isotopes on detrital zircons from sedimentary rocks. Precambr. Res. 222, 368–385.
Wang, W., Wang, F., Chen, F., Zhu, X., Xiao, P., Siebel, W., 2010a. Detrital zircon age and Hf-Nd isotopic composition of Neoproterozoic sedimentary rocks in the Yangtze Block: constraints on the deposition age and provenance. J. Geol. 118, 79–94.
Wang, W., Chen, F., Hu, R., Chu, Y., Yang, Y., 2012a. Provenance and tectonic setting of Neoproterozoic sedimentary sequences in the South China Block: evidence from detrital zircon ages and Hf-Nd isotopes. Int. J. Earth Sci. https://doi.org/10.1007/s00531-011-0746-z.
Wang, W., Zhou, M.F., 2014. Provenance and tectonic setting of the Paleo- to Mesoproterozoic Dongchuan Group in the southwestern Yangtze Block, South China: Implication for the breakup of the supercontinent Columbia. Tectonophysics 610, 110–127.
Wang, W., Zhou, M.F., Yan, D.P., Li, J., 2012b. Depositional age, provenance, and tectonic setting of the Neoproterozoic Sibao Group, southeastern Yangtze Block, South China. Precambr. Res. 192–195, 107–124.
Wang, X.L., Zhou, J.C., Griffin, W.L., Wang, R.C., Qiu, J.S., O'Reilly, S.Y., Xu, X.S., Liu, X.M., Zhang, G.L., 2007a. Detrital zircon geochronology of Precambrian basement sequences in the Jiangnan orogeny: Dating the assembly of the Yangtze and Cathaysia Blocks. Precambr. Res. 159, 117–131.
Wang, Y.J., 1994. Cherts and associated radiolarians in Qinzhou, Guangxi. Chin. Sci. Bull. 39, 1208–1210 (in Chinese).
Wang, Y.J., Fan, W.M., Cawood, P.A., Ji, S.C., Peng, T.P., Chen, X.Y., 2007b. Indosinian high-strain deformationfor the Yunkaidashan tectonic belt, south China: kinematics and 40Ar/39Ar geochronological constraints. Tectonics 26, TC6008. https://doi.org/10.1029/2007TC002099.

Wang, Y.J., Fan, W.M., Zhang, G.W., Zhang, Y.H., 2013a. Phanerozoic tectonics of the SCB: Key observations and controversies. Gondwana Res. 23, 1273–1305.

Wang, J., Li, Z.X., 2003. History of Neoproterozoic rift basins in South China: Implications for Rodinia break-up. Precambr. Res. 122, 141–158.

Wang, Y.J., Zhang, A., Fan, W., Zhao, G., Zhang, G., Zhang, Y., Zhang, F., Li., S., 2011a. Kwangsian crustal anatexis within the eastern South China Block: Geochemical, zircon U-Pb geochronological and Hf isotopic fingerprints from the gneissoid granites of Wugong and Wuyi-Yunkai Domains. Lithos 127, 239–260.

Wang, Y.J., Wu, C.M., Zhang, A.M., Fan, W.M., Zhang, Y.H., Zhang, Y.Z., Peng, T.P., Yin, C.Q., 2012c. Kwangsian and Indosinian reworking of the eastern South China Block: constraints on zircon U-Pb geochronology and metamorphism of amphibolites and granulites. Lithos 150, 227–242.

Wang, Y.J., Zhang, F.F., Fan, W.M., Zhang, G., Chen, S.Y., Cawood, P.A., Zhang, A.M., 2010b. Tectonic setting of the SCB in the early Paleozoic: Resolving intracontinental and ocean closure models from detrital zircon U-Pb geochronology. Tectonics 29, TC6020. https://doi.org/10.1029/2010TC002750.

Wang, Y.J., Zhang, A.M., Cawood, P.A., Fan, W.M., Xu, J.F., Zhang, G.W., Zhang, Y.Z., 2013b. Geochronological, geochemical and Nd-Hf-Os isotopic fingerprinting of an early Neoproterozoic arc-back-arc system in South China and its accretionary assembly along the margin of Rodinia. Precambr. Res. 231, 343–371.

Wu, H.R., 1999. Implications of radiolarian chert for the Palaeogeography of South China. J. Palaeogeogr. 1 (2), 28–35 (in Chinese with English abstract).

Wu, H.R., 2003. Discussion on tectonic Palaeogeography of Nanpanjiang Sea in the late Palaeozoic and Triassic. J. Palaeogeogr. 5 (1), 63–76 (in Chinese with English abstract).

Wu, H.R., Xian, X.Y., Kuang, G.D., et al., 1994a. Late Paleozoic radiolarian chert of South Guangxi and the preliminary discussion on the Tethys of Guangxi. Chin. Sci. Bull. 39 (9), 809–812 (in Chinese).

Wu, H.R., Xian, X.Y., Kuang, G.D., 1994b. Late Paleozoic radiolarian assemblages of southern Guangxi and its geological significance. Scientia Geologica Sinica 29, 339–345 (in Chinese with English abstract).

Wu, G., Zhong, D., Zhang, Q., Ji, J., 1999. Babu-Phu Ngu ophiolities: a geological record of Paleotethyan Ocean bordering China and Vietnam. Gondwana Res. 2 (4), 554–557.

Xia, X.P., Nie, X.S., Lai, C.K., Wang, Y.J., Long, X.P., Meffre, S., 2015. Where was the Ailaoshan Ocean and when did it open: a perspective based on detrital zircon U-Pb age and Hf isotope evidence. Gondwana Res. 36, 488–502.

Xie, C., Zhu, J., Ding, S., Zhang, Y., Fu, T., Li, Z., 2006. Identification of Hercynian shoshonitic intrusive rocks in central Hainan Island and its geotectonic implications. Chin. Sci. Bull. 51, 2507–2519.

Xing, X.W., Wang, Y.J., Zhang, Y.Z., 2016. Detrital zircon U-Pb geochronology and Lu-Hf isotopic compositions of the Wuliangshan metasediment rocks in SW Yunnan (China) and its provenance implications. J. Earth Sci. 27 (3), 412–424.

Xiong, Y.J., Zhang, Z.B., Cai, L.S., Hu, J.J., Zhang, W.M., 1998. Study on the method of the method of the 1:50000 regional geological mapping in continental orogenic belt: an example of Ailaoshan orogenic belt. China University of Geosciences Press, Wuhan (in Chinese with English abstract).

Xu, J., Xia, X.P., Lai, C., Long, X.P., Huang, C., 2019a. When did the Paleotethys Ailaoshan Ocean close: New insights from detrital zircon U-Pb age and Hf isotopes. Tectonics 38, 1798–1823.

Xu, W.C., Luo, B.J., Xu, Y.J., Wang, L., Chen, Q., 2018. Geochronology, geochemistry, and petrogenesis of late Permian to early Triassic mafic rocks from Darongshan, South China: Implications for ultrahigh-temperature metamorphism and S-type granite generation. Lithos 309, 168–180.

Xu, J., Xia, X.P., Huang, C., Cai, K.D., Yin, C.Q., Lai, C.K., 2019b. Changes of provenance of Permian and Triassic sedimentary rocks from the Ailaoshan suture zone (SW China) with implications for the closure of the eastern Paleotethys. J. Asian Earth Sci. 170, 234–248.

Xu, D.R., Xia, B., Li, P.C., Chen, G.H., Ma, C., Zhang, Y.Q., 2007. Protolith natures and U-Pb sensitive high mass-resolution ion microprobe (SHRIMP) zircon ages of the metabasites in Hainan Island, South China: implications for geodynamic evolution since the late Precambrian. Isl. Arc 16, 575–597.

Xu, Y.J., Cawood, P.A., Du, Y.S., 2016. Intraplate orogenesis in response to Gondwana assembly: Kwangsian Orogeny, South China. Am. J. Sci. 316, 329–362.

Xu, Y.J., Cawood, P.A., Du, Y.S., Hu, L.S., 2017. Aulacogen responding to opening of the Ailaoshan Ocean: origin of the Qinfang trough in South China. J. Geol. 125 https://doi.org/10.1086/693036.

Xu, Y.J., Cawood, P.A., Du, Y.S., Hu, L.S., Yu, W.C., Zhu, Y.H., Li, W.C., 2013. Linking south China to northern Australia and India on the margin of Gondwana: Constraints from detrital zircon U-Pb and Hf isotopes in Cambrian strata. Tectonics 32, 1547–1558.

Xu, Y.J., Cawood, P.A., Du, Y.S., Huang, H.W., Wang, X.Y., 2014a. Early Paleozoic orogenesis along Gondwana's northern margin constrained by provenance data from South China. Tectonophysics 636, 40–51.

Xu, Y.J., Cawood, P.A., Du, Y., Zhong, Z., Hughes, N.C., 2014b. Terminal suturing of Gondwana along the southern margin of South China Craton: evidence from detrital zircon U-Pb ages and Hf isotopes in Cambrian and Ordovician strata, Hainan Island. Tectonics 33 (12), 2490–2504.

Xu, X.S., Yin, F.G., Wan, F., Liang, Z.H., Wei, B.D., Zhang, J.D., 2001. The migration of the Qinzhou-Fangcheng trough in Guangxi and associated sedimentary-tectonic transform surfaces. Sedimentary Geol. Tethyan Geol. 21 (4), 1–10 (in Chinese with English abstract).

Xu, X.B., Zhang, Y.Q., Shu, L.S., Jia, D., 2011. LA-ICP-MS U-Pb and 40Ar/39Ar geochronology of the sheared metamorphic rocks in the Wuyishan: constraints on the timing of Early Paleozoic and early Mesozoic tectonic-thermal events in SE China. Tectonophysics 501, 71–86.

Yan, Y.G., Huang, B.C., Zhao, J., Zhang, D.H., Liu, X.H., Charusiri, P., Veeravinantanakul, A., 2017. Large southward motion and clockwise rotation of Indochina throughout the Mesozoic: Paleomagnetic and detrital zircon U-Pb geochronological constraints. Earth Planet. Sci. Lett. 459, 264–278.

Yan, D.P., Zhou, M.F., Wang, C.Y., Xia, B., 2006. Structural and geochronological constraints on the tectonic evolution of the Dulong-Song Chay tectonic dome in Yunnan province, SW China. J. Asian Earth Sci. 28, 332–353.

Yang, J.H., Cawood, P.A., Du, Y.S., Huang, H., Hu, L.S., 2012. Detrital record of Indosinian mountain building in SW China: Provenance of the Middle Triassic turbidites in the Youjiang basin. Tectonophysics 574–575, 105–117.

Yang, J.H., Cawood, P.A., Du, Y.S., Huang, H., Hu, L.S., 2013. A sedimentary archive of tectonic switching from Emeishan Plume to Indosinian orogenic sources in SW China. J. Geol. Soc. 2012–2143.

Yao, W.H., Li, Z.X., 2016. Tectonostratigraphic history of the Ediacaran-Silurian Nanhua foreland basin in South China. Tectonophysics 674, 31–51.

Yao, W.H., Li, Z.X., Li, W.X., Li, X.H., 2017. Proterozoic tectonics of Hainan Island in supercontinent cycles: new insights from geochronological and isotopic results. Precambr. Res. 290, 86–100.

Ye, M.F., Li, X.H., Li, W.X., Liu, Y., Li, Z.X., 2007. SHRIMP zircon U-Pb geochronological and whole-rock geochemical evidence for an early Neoproterozoic Sibaoan magmatic arc along the southeastern margin of the Yangtze Block. Gondwana Res. 12, 144–156.

Yu, J.H., Wang, L., O'Reilly, S., Griffin, W., Zhang, M., Li, C., Shu, L.S., 2009. A Paleoproterozoic orogeny recorded in a long-lived cratonic remnant (Wuyishan terrane), eastern Cathaysia Block, China. Precambr. Res. 174, 347–363.

Yu, J.H., O'Reilly, S.Y., Wang, L., Griffin, W.L., Zhang, M., Wang, R.C., Jiang, S.Y., Shu, L.S., 2008. Where was South China in the Rodinia supercontinent? Evidence from U-Pb geochronology and Hf isotopes of detrital zircons. Precambr. Res. 164, 1–15.

Yu, J.H., O'Reilly, S.Y., Wang, L., Griffin, W.L., Zhou, M.F., Zhang, M., Shu, L., 2010. Components and episodic growth of Precambrian crust in the Cathaysia Block, South China: evidence from U-Pb ages and Hf isotopes of zircons in Neoproterozoic sediments. Precambr. Res. 181, 97–114.

Yu, J.H., Zhou, X., O'Reilly, Y., Zhao, L., Griffin, W.L., Wang, R., Wang, L., Chen, X., 2005. Formation history and protolith characteristics of granulite facies metamorphic rock in Central Cathaysia deduced from U-Pb and Lu-Hf isotopic studies of single zircon grains. Chin. Sci. Bull. 50, 2080–2089.

Yuan, H.L., Gao, S., Dai, M.N., Zong, C.L., Gunther, D., Fontaine, G.H., Liu, X.M., Diwu, C., 2008. Simultaneous determinations of U-Pb age, Hf isotopes and trace element compositions of zircon by excimer laser-ablation quadrupole and multiple-collector ICP-MS. Chem. Geol. 247, 100–118.

Zhang, K.J., Cai, J.X., 2009. NE-SW=trending Hepu-Hetai dextral shear zone in southern China: Penetration of the Yunkai Promontory of South China into Indochina. J. Struct. Geol. 31, 737–748.

Zhang, Y.D., Lenz, A.C., 1998. Early Devonian graptolites from southwest Yunnan. China. J. Paleontol. 72, 353–360.

Zhang, R.Y., Lo, C.H., Li, X.H., Chung, S.L., Anh, T.T., Tri, T.V., 2014. U-Pb dating and tectonic implication of ophiolite and metabasite from the Song Ma suture zone, northern Vietnam. Am. J. Sci. 314, 649–678.

Zhang, N., Xia, W.C., 1998. Time-space distribution of late Paleozoic cherts and evolution of respreading trench in South China. Earth Sci. J. China Univ. Geosci. 23 (4), 124–131 (in Chinese with English abstract).

Zhang, X.C., Wang, Y.J., Clift, P.D., Yan, Y., Zhang, Y.Z., Zhang, L., 2018. Paleozoic tectonic setting and paleogeographic evolution of the Qinfang region, southern South China Block: detrital zircon U-Pb geochronological and Hf isotopic constraints. Geochem. Geophys. Geosyst. https://doi.org/10.1029/2018GC007713.

Zhang, A.M., Wang, Y.J., Fan, W.M., Zhang, Y.Z., Yang, J., 2012. Earliest Neoproterozoic (ca. 1.0 Ga) arc-back-arc-basin nature along the northern Yunkai Domain of the Cathaysia Block: geochronological and geochemical evidence from the metabasite. Precambr. Res. 220–221, 217–233.

Zhang, B.Y., Zhang, H.X., Zhao, Z.H., Yang, S.F., Chen, H.L., Shi, M.Q., 2003. Permian island arc basalt in West Guangdong and East Guangxi tectonic belt, South China: implications for the Paleotethys. J. Nanjing Univ. Nat. Sci. 39 (1), 46–54 (in Chinese with English abstract).

Zhao, G.C., 2015. Jiangnan Orogen in South China: Developing from divergent double subduction. Gondwana Res. 27, 1173–1180.

Zhao, G.C., Cawood, P.A., 2012. Precambrian geology of China. Precambr. Res. 222–223, 13–54. https://doi.org/10.1016/j.precamres.2012.09.017.

Zhao, L., Guo, F., Fan, W.M., Li, C.W., Qin, X.F., Li, H.X., 2010. Crustal evolution of the Shiwandashan area in South China: zircon U-Pb-Hf isotopic records from granulite enclaves in Indo-Sinian granites. Chin. Sci. Bull. 55, 2028–2038.

Zhao, L., Guo, F., Fan, W.M., Li, C.W., Li, H.X., 2012. Origin of the granulite enclaves in Indo-Sinian peraluminous granites, South China and its implication for crustal anataxis. Lithos 126, 248–264.

Zhao, T., Li, J., Liu, G., Cawood, P.A., Zi, J.-W., Wang, K., Feng, Q., Hu, S., Zeng, W., Zhang, H., 2020. Petrogenesis of Archean TTGs and potassic granites in the southern Yangtze Block: Constraints on the early formation of the Yangtze Block. Precambr. Res. 347 https://doi.org/10.1016/j.precamres.2020.105848.

Zhao, X.K., Yong, Z.Q., Li, G.R., Zhang, X.B., Deng, G.J., Li, K., 2007. Residual basin of passive continental margin-a neglected basin type. Oil Gas Geol. 28, 121–128 (in Chinese with English abstract).

Zhao, J.H., Zhou, M.F., Yan, D.P., Zheng, J.P., Li, J.W., 2011. Reappraisal of the ages of Neoproterozoic strata in South China: no connection with the Grenvillian orogeny. Geology 39, 299–302.

Zhong, D.L., Wu, G.Y., Ji, J.Q., Zhang, Q., Ding, L., 1999. Discovery of ophiolites in southeast Yunnan, China. Chin. Sci. Bull. 44, 36–41.

Zhou, Y., Liang, X.Q., Liang, X.R., Jiang, Y., Wang, C., Fu, J.G., Shao, T., 2015. U-Pb geochronology and Hf-isotopes on detrital zircons of Lower Paleozoic strata from Hainan Island: new clues for the early crustal evolution of southeastern South China. Gondwana Res. 27, 1586–1598.
Zhu, D.C., Zhao, Z.D., Niu, Y.L., Dilek, Y., Mo, X.X., 2011. Lhasa terrane in southern Tibet came from Australia. Geology 39, 727–730.
Zi, J.W., Cawood, P.A., Fan, W.M., Tohver, E., Wang, Y.J., McCuaig, T.C., Peng, T.P., 2013. Late Permian-Triassic magmatic evolution in the Jinshajiang orogenic belt, SW China and implications for orogenic processes following closure of the Paleo-Tethys. Am. J. Sci. 313, 81–112.
Zi, J.W., Cawood, P.A., Fan, W.M., Wang, Y.J., Tohver, E., McCuaig, T.C., Peng, T.P., 2012a. Triassic collision in the Paleo-Tethys Ocean constrained by volcanic activity in SW China. Lithos 144–145, 145–160.
Zi, J.W., Cawood, P.A., Fan, W.M., Wang, Y.J., Tohver, E., 2012b. Contrasting rift and subduction-related plagiogranites in the Jinshajiang ophiolitic mélange, southwest China, and implications for the Paleo-Tethys. Tectonics 31, TC2012. https://doi.org/10.1029/2011TC002937.